Geochemistry Geophysics Geosystems G3
AN ELECTRONIC JOURNAL OF THE EARTH SCIENCES
Published by AGU and the Geochemical Society

Article
Volume 1, Number 1
23 February 2000
1008, doi:10.1029/1999GC000018
ISSN: 1525-2027

The $^{40}Ar/^{39}Ar$ age dating of the Madeira Archipelago and hotspot track (eastern North Atlantic)

Jörg Geldmacher, Paul van den Bogaard, Kaj Hoernle, and Hans-Ulrich Schmincke
GEOMAR, Wischhofstrasse, 1-3D-24148, Kiel, Germany (jgeldmacher@ifm-geomar.de)

[1] The $^{40}Ar/^{39}Ar$ ages for 35 volcanic rocks and ^{14}C ages for two charcoal samples from the Madeira Archipelago and Ampère Seamount (eastern North Atlantic) are presented. The volcanic evolution of Madeira can be divided into a voluminous shield stage (>4.6–0.7 Ma) and a subsequent low-volume posterosional stage (<0.7–0 Ma). Volcanism during the shield stage originated from a two-armed rift system, composed of the E–W oriented Madeira rift arm and the N–S oriented Desertas rift arm. Average growth rates for the submarine (5500 km^3/Ma) and subaerial (100–150 km^3/Ma) shield stages on Madeira are among the lowest found for ocean island volcanoes. It is proposed that Madeira represents the present location of a >70 Myr old hotspot which formed Porto Santo Island (11.1–14.3 Ma), Seine, Ampère (31 Ma), Corral Patch and Ormond (65–67 Ma [*Féraud et al.*, 1982, 1986]) Seamounts, and the Serra de Monchique (70–72 Ma [*McIntyre and Berger,* 1982]) complex in southern Portugal. Age and spatial relationships result in a calculated absolute African plate motion above the hotspot of 1.2 cm/yr around a rotation pole located at 43°36′N/ 24°33′W.

Components: 9621 words, 10 figures, 4 tables.

Keywords: Madeira; $^{40}Ar/^{39}Ar$ age dating; hotspot; Desertas Islands; Ampère Seamount; African plate motion.

Index Terms: 1035 Geochronology; 8400 Volcanology; 8157 Tectonophysics: Plate motions: past (3040)

Received 5 October 1999; **Revised** 22 December 1999; **Accepted** 22 December 1999; **Published** 23 February 2000.

Geldmacher, J., P. van den Bogaard, K. Hoernle, and H.-U. Schmincke (2000), The $^{40}Ar/^{39}Ar$ age dating of the Madeira Archipelago and hotspot track (eastern North Atlantic), *Geochem. Geophys. Geosyst.*, *1*, 1008, doi:10.1029/1999GC000018.

1. Introduction

[2] A long-standing question concerns the origin of the ~1700 km belt of volcanism in the eastern North Atlantic located off the coast of Iberia and western Africa between 23° and 38°N (Figure 1)[see *Schmincke*, 1982]. The belt consists of three island groups (Canary, Selvagen, and Madeira Archipelagoes) and more than 20 large seamounts. Global seismic tomographic studies provide evidence for large-scale upwelling from depths of >500 km beneath the region [*Zhang and Tanimoto*, 1992; *Hoernle et al.*, 1995], supporting a mantle plume origin as previously suggested [e.g., *Morgan*, 1972; *Holik and Rabinowitz*, 1991; *Hoernle et al.*, 1991; *Hoernle and Schmincke*, 1993a, b].

[3] The Madeira Archipelago (Figure 2) is located near the southwestern termination of a broad alignment of scattered seamounts and volcanic ridges extending from the Iberian shelf almost 900 km to the southwest (Figure 1). On the basis of its spatial orientation, it has been proposed that this belt of volcanoes could represent a hotspot track [*Morgan*,

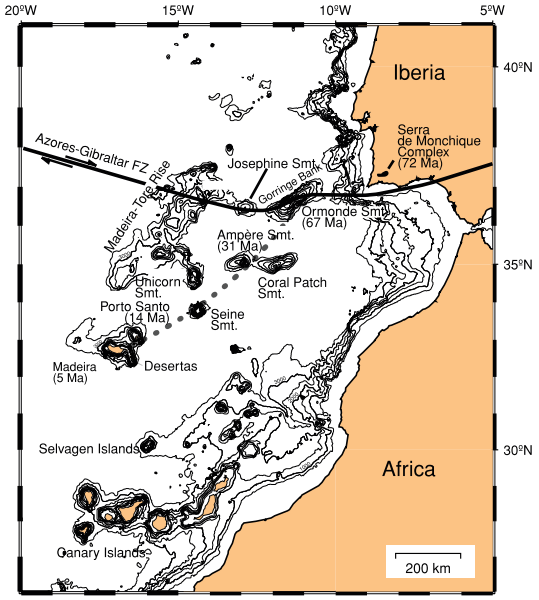

Figure 1. Bathymetric map of seamounts and island groups in the eastern North Atlantic (only depth contours above 3500 m below sea level are shown). Source: TOPEX [*Smith and Sandwell*, 1997]. Azores-Gibraltar Fracture Zone after *Verhbitsky and Zolotarev* [1989]. Proposed Madeira hotspot track shown as thin dotted line (oldest available radiometric ages for each volcano are given in Ma; see text for details).

1981]. Morgan proposes that the trace of this hotspot extends into the Mesozoic, at which time the hotspot was located between Labrador and Greenland. The entire belt can be divided into a western complex of seamounts on the NE–SW trending Madeira-Tore Rise and an eastern chain of large, isolated seamounts forming a slightly curved track toward Madeira Island, which we will henceforth refer to as the Madeira volcanic chain. Gravimetric studies of Josephine Seamount, located at the northern end of the Madeira-Tore rise, have shown that this seamount is in isostatic equilibrium with the underlying oceanic crust, leading to the interpretation that the entire rise structure originated on young lithosphere adjacent to the Mid-Atlantic Ridge [*Peirce and Barton*, 1991]. The eastern chain of isolated volcanoes includes Madeira with the small Desertas Islands, Porto Santo, Seine Seamount, possibly Unicorn Seamount, Ampère Seamount, Coral Patch Seamount, and Ormonde Seamount/Gorringe Bank.

[4] We have undertaken volcanological, geochronological, and geochemical studies on the Madeira Island group and associated seamounts in order to elucidate the origin of the volcanism in the eastern North Atlantic and to constrain the magmatic evolution of the Madeira/Desertas volcanic system. In this study we summarize the results of field studies and present $^{40}Ar/^{39}Ar$ age data from volcanic rocks from the Madeira Island group and Ampère Seamount. The results of geochemical studies will be presented elsewhere (J. Geldmacher and K. Hoernle, manuscript in preparation, 2000).

2. Geological Setting of Islands and Seamounts in the Madeira Chain

2.1. Madeira and Desertas Islands

[5] The Madeira Archipelago consists of five principal islands: the main island of Madeira (728 km^2), the three narrow Desertas Islands (15 km^2) extending more than 60 km SSE of the eastern end of Madeira, and Porto Santo Island (69 km^2) 45 km to the northeast of Madeira (Figure 2). The archipelago is located on 140 Myr old oceanic crust [*Pitman and Talwani*, 1972] and rises from more than 4000 m water depths up to 1862 m above sea level (summit of Pico Ruivo). Previous geological studies [*Carvalho and Brandão*, 1991], geological mapping [*Zbyszewski et al.*, 1973, 1975], and palaeontological work (summarized by *Mitchel-Thomé* [1976]) have outlined a long and complex volcanic history.

[6] Using lithostratigraphic criteria, the geology of Madeira can be divided into four units:

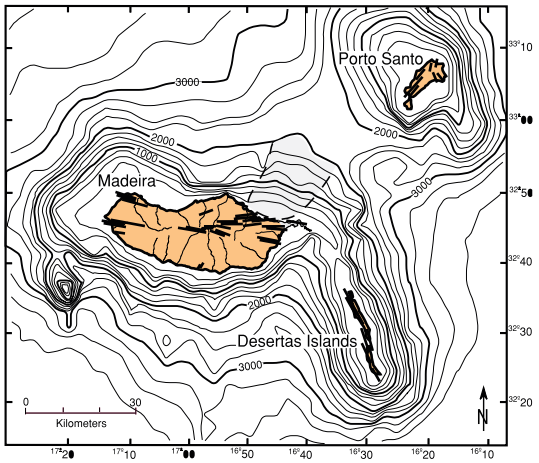

Figure 2. Bathymetric map of the Madeira Archipelago. Source: TOPEX [*Smith and Sandwell*, 1997]. At the eastern tip of Madeira, the E–W oriented Madeira Rift forms an angle of 110° with the narrower NNW–SSE oriented Desertas rift arm. The directions of major dike swarms are shown schematically, as is the location of a postulated sector collapse fan. The seamount SW of Madeira extends to a height of 500 m below sea level and may represent the present location of the Madeira hotspot.

[7] 1. The first is the submarine shield, about which little is known.

[8] 2. The late Miocene to Pliocene basal unit consists primarily of volcanic breccias and pyroclastic deposits with minor lava flows (unit β1 of *Zbyszewski et al.* [1975]). Locally, this unit is extensively cut by dikes which approach dike swarms in some regions, in particular in the central part of the island.

[9] 3. The middle unit is composed primarily of Pliocene to Pleistocene alkalic basalt lava flows (units β 2–4 of *Zbyszewski et al.* [1975]). This unit covers most of the island (Figure 3) and forms lava sequences >500 m in thickness locally cut by dike swarms.

[10] 4. The upper unit consists of scoria cones and intracanyon flows, which were for the most part erupted after considerable erosion of the island.

[11] Published radiometric age data focus on the younger volcanic rocks yielding K/Ar ages ranging from 0.7 to 3 Ma [*Watkins and Abdel-Monem*, 1971; *Ferreira et al.*, 1975; *Féraud et al.*, 1981; *Mata et al.*, 1995] except for two from lava flows with ages of 3.9 Ma [*Ferreira et al.*, 1975] and 4.4 Ma (average of duplicate analyses from *Mata et al.* [1995]). Ages and stratigraphic relationships of the oldest rocks (>3 Ma) are poorly understood. No age or compositional data have been published from the Desertas Islands.

[12] Both Madeira and the Desertas are characterized in their central regions by swarms of steeply dipping, partly sheeted dikes, normal faults and graben structures, and abundant cinder cones stacked one on another. These features are parallel to the long axes of Madeira (E–W) and the Desertas Islands (NNW–SSE) (Figure 2) and are thus characteristic of volcanic rift zones, along which the islands preferably grew by intrusion and extrusion as has been described for rift zones in the Hawaiian and Canary Islands [e.g., *Walker*, 1987; *Carracedo*, 1994]. As seen on a bathymetric map (Figure 2), the Desertas rift builds a 60 km long submarine ridge, rising from more than 4000 m water depths. The Madeira and Desertas rifts form an angle of ~110° and intersect near the eastern tip of Madeira (São Lourenço peninsula). In summary, we consider the Madeira and Desertas ridges to form a single volcanic complex, consisting of an E–W oriented Madeira rift arm and a NNW–SSE oriented Desertas rift arm.

2.2. Porto Santo

[13] Porto Santo is located 45 km to the northeast of Madeira; the two islands are separated by water depths of ~2000 m. Porto Santo is lower in elevation (with its highest peak at 517 m) and more uniform in relief compared to Madeira. A large basaltic to trachytic, mainly submarine, clastic cone makes up the core of the NE part of the island (seamount stage) [*Schmincke and Staudigel*, 1976; R. Schmidt et al., manuscript in preparation, 2000]. Intercalated with the volcanic rocks are shallow water carbonates. The cone is dissected by voluminous trachytic and basaltic intrusions. A thick pile of submarine to subaerial alkali basaltic to hawaiitic lava flows and associated pillows forms the western part of the island. All units are cut by minor trachytic and basaltic intrusions and dikes, which form most hill tops and ridge crests on the island. Dikes show a preferred NE–SW orientation in the western part of the island and a more radial arrangement in the east [*Ferreira and Cotelo Neiva*, 1997]. Published K/Ar ages of Porto Santo range from 12.3 to 13.1 Ma [*Féraud et al.*, 1981].

2.3. Seine, Unicorn, Ampère, and Coral Patch Seamounts

[14] Seine Seamount is located ~200 km NE of Porto Santo, rising from more than 4000 m to less than 200 m water depths. This round seamount has steep sides and a flat top characteristic of a guyot. Unicorn Seamount lies ~100 km due north of Seine Seamount. Ampère and Coral Patch Seamounts are located ~190 km NE of Seine Seamount. Bathymetric data show that the shape of Ampère Seamount is also similar to a guyot with a summit that extends to 59 m below sea level [*Litvin et al.*, 1982; *Marova and Yevsyukov*, 1987]. Alkaline nepheline basaltoids have been described from two short drill holes on the top of the seamount [*Matveyenkov et al.*, 1994]. The neighboring Coral Patch Seamount forms an elongated E–W oriented structure rising up to 900 m below sea level.

2.4. Ormonde Seamount

[15] The 250 km long Gorringe Bank, which lies along the Azores-Gibraltar fracture zone (the Eurasia-African Plate boundary), is dominated by two summits, the Gettysburg (west) and Ormonde (east) Seamounts, which almost reach sea level. Except for the Ormonde summit, the rest of Gorringe Bank consists primarily of altered tholeiitic basalt and serpentinized peridotite [*Auzende et al.*,

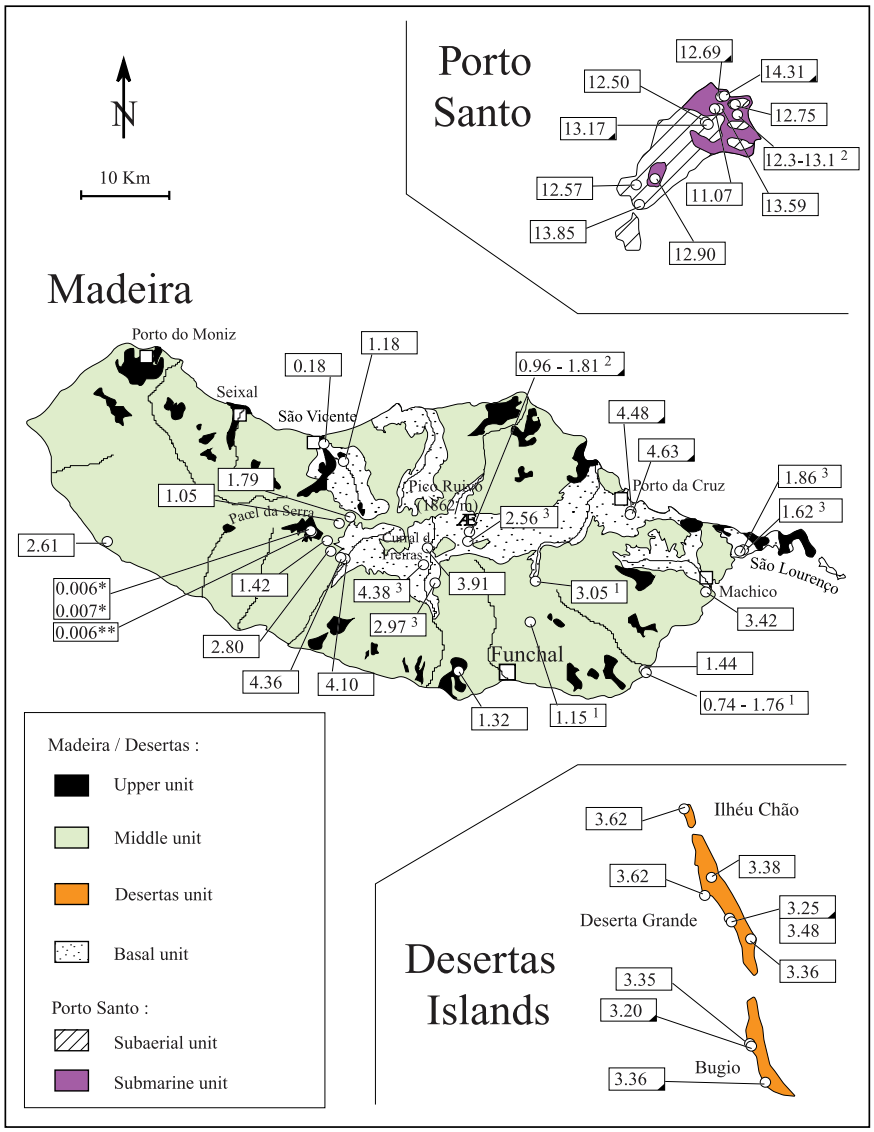

Figure 3. Geological map of Madeira, Desertas, and Porto Santo based on *Zbyszewski et al.* [1975] and *Ferreira and Cotelo Neiva* [1997]. White circles mark sampling sites for age determination.Numbers are in million years. Superscript numbers identify K/Ar dates from (1) *Watkins and Abdel-Monem* [1971], (2) *Féraud et al.* [1981], and (3) *Mata et al.* [1995]. From *Mata et al.* [1995], averages of replicate analyses are shown when replicates are within 2σ error of each other. If not, the age with smallest error is used. Black triangles in the lower right-hand corner of boxes around the ages mark samples from dikes. Numbers with one asterisk are from ^{14}C radiocarbon ages of charcoal from this study and (with two asterisks) *Schmincke* [1998]. All other numbers without superscript indicators are ^{40}Ar/^{39}Ar age determinations from this study.

1978; *Cyagor II Group*, 1984; *Matveyenkov et al.*, 1994] and is considered to be a fragment of oceanic lithosphere of Early Cretaceous age [*Féraud et al.*, 1986] uplifted and slightly tilted along the Azores-Gibraltar fracture zone [*Auzende et al.*, 1978]. In contrast, the younger volcanic rocks on top of Ormonde Seamount comprise a wide range of alkaline rocks, including alkali basalts, nephelinites, and phonolites [*Cornen*, 1982]. The ^{40}Ar/^{39}Ar age dating of Ormonde alkaline volcanic rocks yielded ages between 65 and 67 Ma [*Féraud et al.*, 1982, 1986].

3. Sample Description and Analytical Procedures

[16] Samples from the Madeira archipelago (locations shown in Figure 3) were collected from all stratigraphic units (brief description and sampling sites are given in Table 1). From Madeira Island,

Table 1. Sample Description and Sampling Sites

Sample	Sample Type	Location	Latitude /Longitude
		Madeira	
Ma 85	basanitic lava flow	northern exit of São Vicente village	32°49′08″ 17°02′28″
Ma 19	plag in pumice layer	Street Encumeada-Paul da Serra, between first and second tunnel	32°44′48″ 17°01′32″
Ma 82c	plag in trachyte intrusion	below chapel of São Vicente	32°47′32″ 17°02′00″
Ma 146	plag in pumice layer	behind church of São Martinho	32°38′42″ 16°56′25″
Ma 37	hawaiitic lava flow	Street Encumeada-Paul da Serra, ~1 km behind third tunnel	32°44′11″ 17°02′39″
Ma 107	plag in pumice layer	lower part of road profile of Porto Novo valley (south side)	32°39′31″ 16°48′30″
Ma 75	alkali basaltic sill	quarry near Encumeada pass	32°45′06″ 17°01′07″
Ma 152	alkali basaltic lava flow	road cut east of Jardim do Mar (Rib. Funda valley, near road tunnel)	32°43′48″ 17°11′51″
Ma 44	plag in pumice layer	Street Encumeada-paul da Serra, 0.5 km south of Casa Lombo do Mouro	32°43′50″ 17°03′00″
Ma 170	hawaiitic lava flow	thin flow below lava pile at road cut south part of Machico bay	32°42′32″ 16°45′40″
Ma 227	transitional basalt boulder	road cut at Cumeal village (Cural das Freiras valley)	32°43′58″ 16°57′53″
Ma 208	alkali basaltic lava flow	lower part of eastern slope of Paul da Serra plateau	32°43′37″ 17°02′43″
Ma 203	plag in alkali basaltic flow	lower part of eastern slope of Paul da Serra plateau	32°43′41″ 17°02′47″
13-7-96-1	transitional basalt dike rim	Cruz da Guarda village (south of Porto da Cruz)	32°44′53″ 16°48′42″
13-7-96-3	transitional basalt dike rim	Cruz da Guarda village (south of Porto da Cruz)	32°44′53″ 16°48′42″
		Desertas Islands	
		Ilhéu Chão	
K 22	alkali basaltic lava flow	base of Ilhéu Chão lava flow sequence	32°34′38″ 16°32′27″
		Deserta Grande	
DGR 9	basanitic dike	wall behind big landslide fan near refuge	32°30′35″ 16°30′16″
6302B	megacryst in scoria cone	top plateau near southern end of the island	32°29′38″ 16°29′38″
DGR 47	basanitic lava flow	Pedregal summit	32°32′23″ 16°31′21″
DGR 2	alkali basaltic lava flow	base of lava flow sequence (south of refuge)	32°30′30″ 16°30′19″
K 31	alkali basalti lava flow	base of lava flow sequence, shore just south of Ponta do Pedregal	32°31′55″ 16°31′23″
		Ilhéu do Bugio	
K 15	alkali basaltic dyke	shore near Canto do Furado	32°25′56″ 16°29′17″
K 5	plag in alkali basaltic dyke	shore near Ponta da Estância	32°24′24″ 16°28′27″
K 11	alkali basaltic beach block	shore near Canto do Furado	32°25′56″ 16°29′17″

Table 1. (Continued)

Sample	Sample Type	Location	Latitude /Longitude
		Porto Santo	
K 43	basanitic intrusion	near Pico Juliana summit	33°05′23″ 16°19′09″
K 38	plag in trachytic intrusion	west slope of Pico Castelo (above airport)	33°04′44″ 16°19′51″
K 67a	alkali basaltic dike	ridge of Espigao summit	33°02′24″ 16°22′52″
K 48	alkali basaltic dike	street between Serra de Dentro and Camacha (below small quarry west of Pico Branco)	33°05′29″ 16°18′36″
K 47	plag in trachytic intrusion	street between Serra de Dentro and Camacha (small quarry west of Pico Branco)	33°05′26″ 16°18′23″
K 68	rachytic intrusion	near ana Ferreira Summit	33°02′27″ 16°18′51″
K 42	plag in benmoreitic dike	west slope of Pico Castelo (above airport)	33°04′47″ 16°19′42″
K 46	plag in basanitic intrusion	below Pico Juliana summit	33°05′26″ 16°19′02″
K 55	alkali basaltic lava flow	lower part of lava flow sequence at Zimbralinho bay (sw part of the island)	33°01′49″ 16°22′57″
K 49	plag in benmoreitic dike	street between Serra de Dentro and Camacha (ne of Pico Juliana)	33°05′29″ 16°18′40″
		Ampére Seamount	
DS 797-1	hawaiitic beach cobble	eastern part of summit at 35°03′n/12°54″w (160m water depth)	35°03′02″ 12°54′00″

five samples from the basal unit, eight samples from the middle unit, and two samples from the upper unit were dated. At the center of Madeira, a continuous section was sampled, extending from the basal unit through the middle and upper units on the eastern slope of Paul da Serra plateau (Figures 4 and 5). Desertas's samples comprise rocks from the upper and lower parts of the successions of all three islands. On Porto Santo, samples were taken from the NE and SW parts of the island and come from all stratigraphic units.

[17] Rock samples from Madeira and Desertas islands chosen for age dating range from tholeiites to alkali basalt to basanite and hawaiite. Olivine is the dominant phenocryst phase. Ti-augite and/or plagioclase also occur as phenocrysts. The groundmass consists of plagioclase, Ti-augite, olivine, and Fe/Ti-oxides. Two glass samples from tholeiitic dike rims from the basal unit on Madeira were also dated. Six samples of plagioclase crystals were separated from thin trachytic pumice deposits and from one small rhyolitic intrusion. In contrast to Madeira and the Desertas, differentiated rocks are more common on Porto Santo. Plagioclase crystals from Porto Santo were separated from two benmoreitic dikes and two trachytic intrusions. Whole rock samples range from basanites to trachytes. Ampère Seamount sample DS 797-1 is a rounded beach cobble of hawaiitic composition and was recovered during F.S. *Poseidon* cruise 235. Descriptions and locations of land and dredge samples are compiled in Table 1.

[18] Following removal of altered surfaces, pieces of selected rock samples were crushed in a jaw crusher to <1 mm and <0.5 mm size and sieved. Matrix chips, fresh glass, or plagioclase phenocrysts were hand-picked under a binocular microscope and cleaned with distilled H_2O in an ultrasonic disintegrator. Plagioclase crystals (250–1000 μm) were treated in 5% HF for 5 min. Plagioclase crystals and rock matrix chip samples were placed in drill holes in 99.95% pure aluminum disks. Sample disks with a three-dimensional array of 27.92 Ma TCR (batch 85G003) sanidine monitor [*Duffield and Dalrymple*, 1990] were secured together, sealed in an aluminum can, and irradiated with 1 mm Cd shielding at the Geesthacht Research Center (Germany). *J* values and associated errors were interpolated for each sample position using a three-dimensional least squares cosine plane fit. The $^{40}Ar/^{39}Ar$ laser total fusion analyses were conducted at the Geomar Geochronology Laboratory using a 25 W Spectra Physics argon ion laser and a MAP 216 series mass

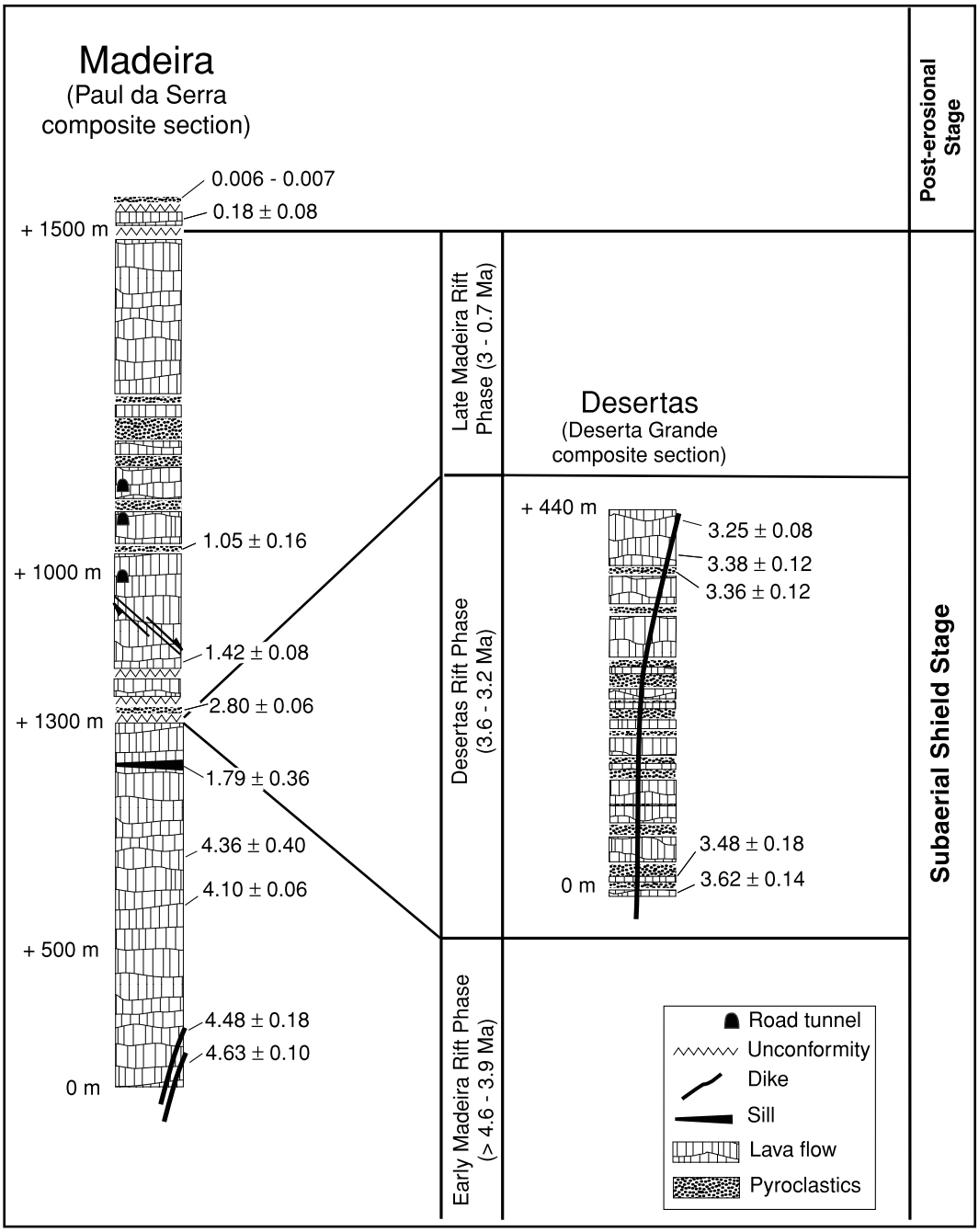

Figure 4. Stratigraphic sections are shown for Paul da Serra on (left) Madeira and (right) Deserta Grande summarizing the subaerial evolution of the Madeira/Desertas volcanic system. Elevations are given in meters above sea level (note that Paul da Serra profile is a composite section). All ages are in million years with 2σ errors. The ^{14}C radiocarbon ages are calibrated to B.P.

spectrometer fitted with a Baur-Signer ion source and a Johnson electron multiplier. Between 5 and 13 single grains (rock/glass fragments or plagioclase crystals) of each sample were completely fused (see Tables 2 and 3 for number of single particles analyzed). Raw mass spectrometer peaks were corrected for mass discrimination, background values (determined between every 4 or 5 analyses), and interfering neutron reactions on Ca and K using optical grade CaF_2 and K_2SO_4 salts that had been irradiated together with the samples. Age uncertainties were calculated by partial differentiation of the age equation [*Dalrymple and Duffield*, 1988] and include uncertainties in the

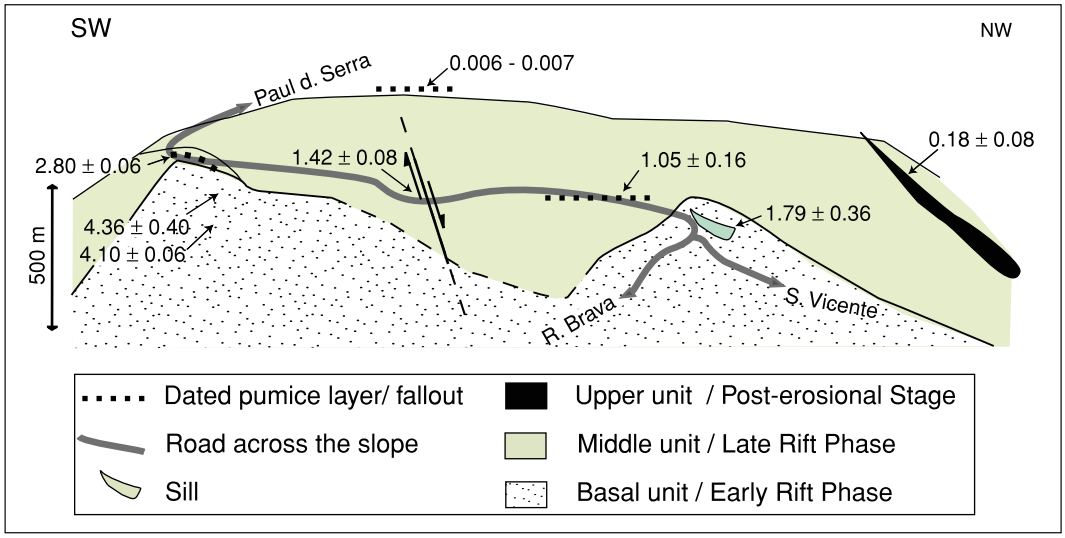

Figure 5. Schematic outcrop sketch of Paul da Serra profile (eastern slope) in central Madeira. Encumeada pass is at the road junction at the right. All ages are in million years.

determination of the flux monitor, *J*, the blank determination, the regression of the intensities of the individual isotopes, and the mass discrimination correction (1.0083 per AMU). Ages and error estimates were determined by calculating the mean apparent age of each population (single fusion ages weighted by the inverse of their variance following the method described by *Young* [1962]), assuming an initial "atmospheric" $^{40}Ar/^{39}Ar$ ratio of 295.5. Isochrons have been calculated as inverse isochrons using *York*'s [1969] least squares fit that accommodates errors in both ratios and correlation of errors. Mean squared weighted deviates (MSWD) were determined for the mean apparent ages and isochron ages in order to test the scatter of the single fusion data [*Wendt and Carl*, 1991]. If the scatter was greater than predicted from the analytical uncertainties (MSWD > 1), the analytical error has been expanded by multiplying by the square root of the MSWD [*York*, 1969]. Errors are quoted at the 2σ level. Mean apparent ages, isochron ages, and mean square weighted deviates are reported in Table 1. Because of the reasonably good control of the initial $^{40}Ar/^{36}Ar$ ratios in isotope correlation diagrams (see Figures 6, 7, and 8), inherited or excess ^{40}Ar can be ruled out for samples within 2σ error from the accepted initial value of 295.5 or slightly lower. If the isotope correlation gives atmospheric initial Ar isotope ratios (within error), a relatively inaccurate determination of the initial ratio for the isochron age would tend to adulterate rather than to improve the absolute age. Therefore, except for sample K 48, the mean apparent age is accepted instead of the isochron age to represent the age of crystallization. Because sample K 48 has an elevated initial $^{40}Ar/^{36}Ar$ ratio (outside of 2σ error from the accepted value), the isochron age is accepted for this sample instead of the apparent age.

[19] Two samples of charcoal, at the base of a pyroclastic fallout deposit on top of Paul da Serra plateau on Madeira, were selected for radiocarbon dating (Table 4). Samples were leached in 1% HCL, 1% NaOH, and again with 1% HCL at 60°C. The graphitisized samples were analyzed for ^{14}C ratios with an accelerator mass spectrometer (AMS) at the Leibniz Laboratory at Christian Albrechts University in Kiel. The measured ^{14}C ratios are corrected for mass fractionation and converted into calibrated age after *Stuiver and Reimerm* [1993].

4. Results

4.1. Madeira

[20] The oldest dated rocks on Madeira occur in the vicinity of Porto da Cruz (NE Madeira, Figure 3). Fresh glass rims of tholeiitic dikes, cross-cutting volcanic breccia and pyroclastic rocks, gave $^{40}Ar/^{39}Ar$ ages of 4.48 ± 0.18 and 4.63 ± 0.10 Ma (samples 13-7-96-1 and 13-7-96-3). Lavas from the basal unit in Curral das Freiras valley and near the base of the eastern slope of Paul da Serra plateau (Figure 4) produced ages between 3.9 and 4.4 Ma (MA 227, MA 208, MA 203). Only one flow from Madeira dated in this study has an age between 2.8 and 3.9 Ma. Sample MA 170, with

Table 2. Analytical Results

Sample	Mass, mg	$40^{*39}K$ 1σ	$^{40}Ar_{atm}$%	CA/K 1σ	Apparent Age 1σ
		MA107: J = 0.00221926 ± 0.00000402			
MA107	2.19E−01	3.806E−01 ± 1.01E−01	70.2	3.81 ± 0.01	1.52E+06 ± 4.0E+05
MA107	2.34E+00	3.597E−01 ± 1.29E−02	74.7	4.66 ± 0.00	1.44E+06 ± 5.2E+04
MA107	6.22E−01	3.637E−01 ± 3.48E−02	93.7	5.42 ± 0.01	1.46E+06 ± 1.4E+05
MA107	1.05E+00	3.440E−01 ± 2.16E−02	90.3	4.84 ± 0.01	1.38E+06 ± 8.7E+04
MA107	9.09E−01	3.834E−01 ± 3.63E−02	80.0	5.74 ± 0.01	1.53E+06 ± 1.5E+05
MA107	5.75E−01	3.864E−01 ± 6.12E−02	92.2	5.94 ± 0.01	1.55E+06 ± 2.4E+05
MA107	4.80E−01	3.810E−01 ± 4.43E−02	93.2	4.75 ± 0.01	1.52E+06 ± 1.8E+05
MA107	4.89E−01	2.425E−01 ± 5.81E−02	95.8	6.28 ± 0.01	9.71E+05 ± 2.3E+05
MA107	1.12E+00	3.854E−01 ± 2.26E−02	63.9	4.19 ± 0.01	1.54E+06 ± 9.0E+04
MA107	4.16E−01	3.992E−01 ± 6.63E−02	79.6	6.45 ± 0.02	1.60E+06 ± 2.7E+05
MA107	6.97E−01	3.933E−01 ± 3.89E−02	80.3	6.41 ± 0.01	1.57E+06 ± 1.6E+05
MA107	4.58E−01	4.464E−01 ± 6.05E−02	74.4	3.50 ± 0.01	1.79E+06 ± 2.4E+05
MA107	4.10E−01	4.337E−01 ± 6.01E−02	81.5	3.58 ± 0.01	1.74E+06 ± 2.4E+05
		MA146: J = 0.0021094 ± 0.000004706			
MA146	6.98E−01	5.333E−01 ± 1.21E−01	73.4	35.47 ± 0.07	2.03E+06 ± 4.6E+05
MA146	2.66E−01	6.294E−01 ± 2.76E−01	74.4	32.98 ± 0.15	2.39E+06 ± 1.0E+06
MA146	5.82E−01	6.081E−01 ± 1.57E−01	78.5	33.08 ± 0.10	2.31E+06 ± 6.0E+05
MA146	4.88E−01	3.094E−01 ± 1.45E−01	92.4	34.29 ± 0.07	1.18E+06 ± 5.5E+05
MA146	5.26E−01	4.437E−01 ± 1.50E−01	78.5	35.19 ± 0.08	1.69E+06 ± 5.7E+05
MA146	2.92E−01	6.358E−01 ± 3.31E−01	77.5	35.02 ± 0.18	2.42E+06 ± 1.3E+06
MA146	1.11E+00	3.847E−01 ± 5.72e −02	76.7	39.41 ± 0.07	1.46E+06 ± 2.2E+05
MA146	2.76E−01	5.979E−01 ± 2.61E−01	82.6	36.48 ± 0.17	2.27E+06 ± 9.9E+05
MA146	2.49E−01	3.410E−01 ± 2.52E−01	89.7	34.12 ± 0.11	1.30E+06 ± 9.6E+05
MA146	3.49E−01	3.285E−01 ± 1.77E−01	84.9	33.09 ± 0.12	1.25E+06 ± 6.7E+05
		MA19: J = 0.0021094 ± 0.000004706			
MA19	3.10E−01	2.832E−01 ± 1.04E−01	86.5	21.96 ± 0.07	1.08E+06 ± 3.9E+05
MA19	1.43E+00	2.662E−01 ± 6.68E−02	40.5	22.11 ± 0.03	1.01E+06 ± 2.5E+05
MA19	9.35E−01	3.053E−01 ± 5.28E−02	52.3	21.05 ± 0.05	1.16E+06 ± 2.0E+05
MA19	8.85E−01	2.729E−01 ± 4.86E−02	42.5	20.78 ± 0.05	1.04E+06 ± 1.8E+05
MA19	7.74E−01	3.853E−01 ± 6.92E−02	27.2	29.01 ± 0.08	1.47E+06 ± 2.6E+05
MA19	6.76E−01	3.330E−01 ± 7.06E−02	36.3	21.07 ± 0.06	1.27E+06 ± 2.7E+05
MA19	6.29E−01	3.471E−01 ± 5.27E−02	25.4	18.05 ± 0.04	1.32E+06 ± 2.0E+05
MA19	4.67E−01	3.094E−01 ± 4.31E−02	44.4	19.80 ± 0.05	1.18E+06 ± 1.6E+05
MA19	4.24E−01	5.308E−01 ± 9.88E−02	2.7	22.59 ± 0.06	2.02E+06 ± 3.8E+05
MA19	3.79E−01	4.991E−01 ± 5.36E−02	5.4	22.48 ± 0.07	1.90E+06 ± 2.0E+05
MA19	3.32E−01	5.835E−01 ± 1.54E−01	6.2	27.26 ± 0.08	2.22E+06 ± 5.8E+05
		MA44: J = 0.00221926 ± 0.00000402			
MA44	2.02E−01	7.907E−01 ± 7.72E−02	39.6	1.80 ± 0.01	3.16E+06 ± 3.1E+05
MA44	8.16E−01	7.010E−01 ± 3.89E−02	77.7	4.30 ± 0.01	2.80E+06 ± 1.6E+05
MA44	1.79E+00	6.927E−01 ± 2.54E−02	83.8	1.65 ± 0.00	2.77E+06 ± 1.0E+05
MA44	1.65E+00	6.981E−01 ± 1.63E−02	84.8	1.82 ± 0.00	2.79E+06 ± 6.5E+04
MA44	8.26E−01	6.922E−01 ± 3.54E−02	89.3	1.49 ± 0.00	2.77E+06 ± 1.4E+05
MA44	6.42E−01	6.816E−01 ± 4.52E−02	89.0	2.01 ± 0.01	2.73E+06 ± 1.8E+05
MA44	9.74E−01	7.368E−01 ± 1.46E−02	40.0	2.03 ± 0.00	2.95E+06 ± 5.9E+04
MA44	1.11E+00	7.553E−01 ± 1.62E−02	47.4	1.97 ± 0.00	3.02E+06 ± 6.5E+04
MA44	5.06E−01	7.790E−01 ± 2.84E−02	71.3	1.91 ± 0.01	3.12E+06 ± 1.1E+05
MA44	1.47E+00	7.533E−01 ± 1.64E−02	51.1	3.57 ± 0.01	3.01E+06 ± 6.6E+04
MA44	3.46E−01	7.218E−01 ± 3.92E−02	60.8	1.74 ± 0.01	2.89E+06 ± 1.6E+05
		MA82c: J = 0.0021094 ± 0.000004706			
MA82c	2.54E−01	3.261E−01 ± 5.53E−02	67.3	3.00 ± 0.01	1.24E+06 ± 2.1E+05
MA82c	6.18E−01	3.283E−01 ± 2.55E−02	70.7	5.05 ± 0.01	1.25E+06 ± 9.7E+04
MA82c	5.74E−01	3.444E−01 ± 3.76E−02	72.8	3.58 ± 0.01	1.31E+06 ± 1.4E+05
MA82c	8.14E−01	3.153E−01 ± 2.20E−02	77.1	4.21 ± 0.01	1.20E+06 ± 8.4E+04
MA82c	4.75E−01	2.908E−01 ± 5.86E−02	78.4	3.75 ± 0.01	1.11E+06 ± 2.2E+05
MA82c	4.94E−01	3.193E−01 ± 4.67E−02	85.3	5.20 ± 0.01	1.21E+06 ± 1.8E+05
MA82c	3.14E−01	2.677E+00 ± 3.52E+00	94.9	4.57 ± 0.15	1.02E+07 ± 1.3E+07
MA82c	4.42E−01	3.123E−01 ± 8.26E−02	87.9	5.77 ± 0.02	1.19E+06 ± 3.1E+05

Table 2. (continued)

Sample	Mass, mg	$40^{*39}K$ 1σ	$^{40}Ar_{atm}$%	CA/K 1σ	Apparent Age 1σ
MA82c	2.02E−01	1.228E−01 ± 9.97E−02	96.7	5.34 ± 0.03	4.67E+05 ± 3.8E+05
MA82c	2.19E−01	2.394E−01 ± 8.25E−02	88.5	3.31 ± 0.01	9.11E+05 ± 3.1E+05
		797-1: J = 0.00103666 ± 0.00000268			
797-1	2.76E−01	1.688E+01 ± 1.59E−01	61.0	5.79 ± 0.02	3.13E+07 ± 3.0E+05
797-1	2.82E−01	1.688E+01 ± 1.85E−01	57.4	5.14 ± 0.02	3.13E+07 ± 3.5E+05
797-1	3.04E−01	1.679E+01 ± 1.68E−01	57.5	6.12 ± 0.04	3.11E+07 ± 3.2E+05
797-1	3.88E−01	1.681E+01 ± 1.28E−01	57.8	5.57 ± 0.03	3.12E+07 ± 2.5E+05
797-1	1.86E−01	1.718E+01 ± 1.08E−01	51.1	4.62 ± 0.03	3.18E+07 ± 2.1E+05
797-1	4.80E−01	1.676E+01 ± 8.08E−02	57.6	5.21 ± 0.02	3.11E+07 ± 1.7E+05
797-1	2.31E−01	1.685E+01 ± 1.47E−01	55.3	4.53 ± 0.22	3.12E+07 ± 2.8E+05
797-1	2.20E−01	1.659E+01 ± 1.46E−01	64.7	5.13 ± 0.44	3.08E+07 ± 2.8E+05
797-1	2.65E−01	1.649E+01 ± 3.77E−01	66.3	5.54 ± 0.53	3.06E+07 ± 7.0E+05
797-1	2.01E−01	1.635E+01 ± 4.43E−01	72.2	3.89 ± 0.70	3.03E+07 ± 8.2E+05
797-1	2.09E−01	1.691E+01 ± 3.00E−01	64.0	4.79 ± 0.46	3.13E+07 ± 5.6E+05
797-1	1.92E−01	1.728E+01 ± 3.29E−01	54.3	6.58 ± 0.38	3.20E+07 ± 6.1E+05
797-1	1.94E−01	1.687E+01 ± 2.31E−01	57.9	4.92 ± 0.32	3.13E+07 ± 4.3E+05
		K42: J = 0.0010318 ± 0.000002035			
K42	3.55E−01	7.574E+00 ± 5.69E−01	36.9	30.54 ± 0.17	1.40E+07 ± 1.1E+06
K42	5.80E−01	7.274E+00 ± 3.62E−01	53.7	30.79 ± 0.09	1.35E+07 ± 6.7E+05
K42	2.00E−01	7.586E+00 ± 1.19E+00	58.7	55.92 ± 0.54	1.41E+07 ± 2.2E+06
K42	1.60E−01	7.220E+00 ± 1.97E+00	70.8	71.20 ± 0.72	1.34E+07 ± 3.6E+06
K42	3.16E−01	7.628E+00 ± 4.65E−01	57.0	29.01 ± 0.12	1.41E+07 ± 8.6E+05
K42	2.61E−01	6.530E+00 ± 1.11E+00	49.6	72.23 ± 0.38	1.21E+07 ± 2.0E+06
K42	3.58E−01	7.059E+00 ± 4.96E−01	60.8	31.84 ± 0.19	1.31E+07 ± 9.2E+05
K42	3.78E−01	6.995E+00 ± 9.03E−01	87.6	60.33 ± 0.36	1.30E+07 ± 1.7E+06
K42	8.58E−01	7.420E+00 ± 2.29E−01	52.8	26.33 ± 0.12	1.38E+07 ± 4.2E+05
K42	9.91E−01	7.362E+00 ± 4.08E−01	83.9	35.63 ± 0.11	1.37E+07 ± 7.5E+05
K42	1.11E+00	6.263E+00 ± 2.58E−01	76.1	50.15 ± 0.20	1.16E+07 ± 4.8E+05
		K46: J = 0.00103451 ± 0.00000196			
K46	3.10E−01	1.044E+01 ± 2.29E+00	84.7	196.5 ± 1.89	1.94E+07 ± 4.2E+06
K46	2.74E−01	9.205E+00 ± 1.16E+00	24.5	76.47 ± 0.53	1.71E+07 ± 2.1E+06
K46	7.88E−01	6.730E+00 ± 3.58E−01	72.0	86.92 ± 0.43	1.25E+07 ± 6.6E+05
K46	8.13E−01	7.815E+00 ± 3.30E−01	70.0	88.25 ± 0.43	1.45E+07 ± 6.1E+05
K46	5.80E−01	7.501E+00 ± 3.97E−01	66.7	71.38 ± 0.32	1.39E+07 ± 7.4E+05
K46	7.58E−01	6.957E+00 ± 3.22E−01	73.8	71.80 ± 0.34	1.29E+07 ± 6.0E+05
K46	5.50E−01	7.621E+00 ± 4.65E−01	22.8	82.84 ± 0.47	1.42E+07 ± 8.6E+05
K46	3.01E−01	7.310E+00 ± 2.42E−01	29.5	12.58 ± 0.09	1.36E+07 ± 4.5E+05
K46	3.50E−01	6.809E+00 ± 7.17E−01	62.6	72.46 ± 0.45	1.27E+07 ± 1.3E+06
K46	2.82E−01	6.037E+00 ± 1.95E+00	84.0	188.6 ± 2.50	1.12E+07 ± 3.6E+06
		K49: J = 0.0010318 ± 0.000002035			
K49	3.13E−01	7.966E+00 ± 3.06E−01	23.2	8.73 ± 0.04	1.48E+07 ± 5.6E+05
k49	4.05E−01	7.922E+00 ± 6.29E−01	64.6	38.15 ± 0.20	1.47E+07 ± 1.2E+06
K49	3.20E−01	7.682E+00 ± 1.48E−01	24.2	6.14 ± 0.04	1.42E+07 ± 2.8E+05
K49	3.99E−01	7.958E+00 ± 2.36E−01	44.0	14.21 ± 0.07	1.48E+07 ± 4.4E+05
k49	2.99E−01	6.638E+00 ± 5.91E−01	60.5	38.42 ± 0.20	1.23E+07 ± 1.1E+06
K49	3.67E−01	7.817E+00 ± 1.11E−01	19.5	5.77 ± 0.02	1.45E+07 ± 2.1E+05
k49	3.72E−01	7.222E+00 ± 9.73E−01	87.2	43.45 ± 0.21	1.34E+07 ± 1.8E+06
K49	5.31E−01	7.566E+00 ± 4.77E−01	81.9	26.82 ± 0.11	1.40E+07 ± 8.8E+05
K49	6.12E−01	6.745E+00 ± 5.85E−01	88.0	43.44 ± 0.15	1.25E+07 ± 1.1E+06
K49	1.56E+00	7.727E+00 ± 1.41E−01	68.9	20.41 ± 0.04	1.43E+07 ± 2.6E+05
K49	1.24E+00	7.595E+00 ± 1.27E−01	55.7	18.49 ± 0.05	1.41E+07 ± 2.4E+05
		K55: J = 0.00103451 ± 0.00000196			
K55	2.04E−01	6.653E+00 ± 2.51E−01	74.2	6.71 ± 0.03	1.24E+07 ± 4.7E+05
K55	3.41E−01	7.685E+00 ± 1.23E−01	76.0	6.74 ± 0.04	1.43E+07 ± 2.3E+05
K55	2.28E−01	7.503E+00 ± 2.45E−01	71.3	6.78 ± 0.04	1.39E+07 ± 4.5E+05
K55	2.35E−01	7.281E+00 ± 2.38E−01	75.9	7.10 ± 0.04	1.35E+07 ± 4.4E+05
K55	9.61E−01	7.496E+00 ± 7.65E−02	74.3	6.64 ± 0.01	1.39E+07 ± 1.4E+05

Table 2. (continued)

Sample	Mass, mg	40*^{39}K 1σ	$^{40}Ar_{atm}$%	CA/K 1σ	Apparent Age 1σ
K55	4.14E−01	7.195E+00 ± 1.53E−01	78.0	7.55 ± 0.03	1.34E+07 ± 2.8E+05
K55	4.70E−01	7.514E+00 ± 1.70E−01	71.6	7.30 ± 0.03	1.40E+07 ± 3.2E+05
		K48: J = 0.00103451 ± 0.00000196			
K48	3.40E−01	7.586E+00 ± 2.97E−01	70.6	12.49 ± 0.04	1.41E+07 ± 5.5E+05
K48	2.39E−01	7.498E+00 ± 3.15E−01	63.1	12.77 ± 0.05	1.39E+07 ± 5.8E+05
K48	8.23E−01	9.845E+00 ± 1.71E−01	85.9	13.63 ± 0.03	1.83E+07 ± 3.2E+05
K48	9.40E−01	8.167E+00 ± 8.10E−02	78.5	12.69 ± 0.03	1.52E+07 ± 1.5E+05
K48	9.26E−01	8.565E+00 ± 1.35E−01	83.9	13.57 ± 0.03	1.59E+07 ± 2.5E+05
K48	9.08E−01	7.994E+00 ± 8.99E−02	74.5	12.65 ± 0.04	1.49E+07 ± 1.7E+05
		K47: J = 0.0010318 ± 0.000002035			
K47	3.25E−01	6.013E+00 ± 4.38E−01	30.8	33.53 ± 0.27	1.12E+07 ± 8.1E+05
K47	4.10E−01	6.664E+00 ± 3.13E−01	17.7	25.33 ± 0.12	1.24E+07 ± 5.8E+05
K47	2.40E−01	7.093E+00 ± 5.55E−01	24.9	25.48 ± 0.12	1.32E+07 ± 1.0E+06
K47	3.15E−01	7.036E+00 ± 3.72E−01	26.1	26.42 ± 0.17	1.30E+07 ± 6.9E+05
K47	2.58E−01	6.420E+00 ± 8.73E−01	47.9	22.08 ± 0.23	1.19E+07 ± 1.6E+06
K47	7.18E−01	6.925E+00 ± 1.36E−01	31.1	14.21 ± 0.06	1.28E+07 ± 2.5E+05
K47	6.33E−01	7.126E+00 ± 2.17E−01	17.5	25.75 ± 0.08	1.32E+07 ± 4.0E+05
K47	6.64E−01	6.730E+00 ± 2.19E−01	21.8	22.00 ± 0.10	1.25E+07 ± 4.1E+05
K47	6.56E−01	6.895E+00 ± 2.98E−01	17.2	32.29 ± 0.11	1.28E+07 ± 5.5E+05
K47	6.23E−01	6.825E+00 ± 1.54E−01	47.7	21.97 ± 0.10	1.27E+07 ± 2.9E+05
K47	1.43E+00	6.927E+00 ± 1.58E−01	7.6	29.49 ± 0.11	1.28E+07 ± 2.9E+05
		K67a: J = 0.0010318 ± 0.000002035			
K67a	2.56E−01	7.289E+00 ± 4.16E−01	36.5	23.77 ± 0.10	1.35E+07 ± 7.7E+05
K67a	6.61E−01	6.733E+00 ± 9.07E−02	29.8	13.43 ± 0.02	1.25E+07 ± 1.7E+05
K67a	3.75E−01	6.825E+00 ± 1.84E−01	35.0	29.60 ± 0.10	1.27E+07 ± 3.4E+05
K67a	5.72E−01	6.744E+00 ± 5.89E−02	48.9	7.85 ± 0.04	1.25E+07 ± 1.1E+05
K67a	4.77E−01	6.662E+00 ± 1.22E−01	44.9	8.85 ± 0.04	1.24E+07 ± 2.3E+05
K67a	7.46E−01	6.778E+00 ± 4.71E−02	23.9	5.94 ± 0.02	1.26E+07 ± 9.1E+04
K67a	9.13E−01	6.878E+00 ± 1.26E−01	52.2	19.53 ± 0.05	1.28E+07 ± 2.3E+05
K67a	4.10E−01	6.972E+00 ± 1.35E−01	46.8	12.92 ± 0.06	1.29E+07 ± 2.5E+05
		K68: J = 0.0010318 ± 0.000002035			
K68	1.94E−01	6.996E+00 ± 7.45E−02	23.6	1.16 ± 0.01	1.30E+07 ± 1.4E+05
K68	1.61E−01	6.911E+00 ± 9.12E−02	23.4	1.02 ± 0.01	1.28E+07 ± 1.7E+05
K68	2.54E−01	6.978E+00 ± 7.87E−02	21.9	1.13 ± 0.00	1.29E+07 ± 1.5E+05
K68	4.17E−01	6.965E+00 ± 4.27E−02	22.6	1.17 ± 0.01	1.29E+07 ± 8.3E+04
K68	2.62E−01	7.058E+00 ± 6.48E−02	27.2	1.14 ± 0.01	1.31E+07 ± 1.2E+05
K68	3.05E−01	6.891E+00 ± 5.90E−02	22.9	1.10 ± 0.01	1.28E+07 ± 1.1E+05
K68	3.97E−01	6.920E+00 ± 4.24E−02	22.5	1.10 ± 0.01	1.28E+07 ± 8.2E+04
		137-1: J =0.00103666 ± 0.00000268			
13-7-96-1	2.90E−01	2.443E+00 ± 2.45E−01	76.7	14.52 ± 0.04	4.56E+06 ± 4.6E+05
13-7-96-1	5.40E−01	2.377E+00 ± 1.17E−01	86.2	14.51 ± 0.05	4.44E+06 ± 2.2E+05
13-7-96-1	1.52E+00	2.325E+00 ± 8.40E−02	87.7	14.58 ± 0.02	4.34E+06 ± 1.6E+05
13-7-96-1	8.09E−01	2.550E+00 ± 9.39E−02	77.4	14.65 ± 0.02	4.76E+06 ± 1.8E+05
13-7-96-1	6.95E−01	2.307E+00 ± 1.03E−01	55.5	14.60 ± 0.05	4.31E+06 ± 1.9E+05
13-7-96-1	4.60E−01	2.345E+00 ± 9.95E−02	83.6	14.68 ± 0.04	4.38E+06 ± 1.9E+05
13-7-96-1	4.38E−01	2.704E+00 ± 1.87E−01	80.0	14.58 ± 0.07	5.05E+06 ± 3.5E+05
		137-3: J = 0.00103666 ± 0.00000268			
13-7-96-3	1.55E+00	2.492E+00 ± 5.46E−02	45.2	14.55 ± 0.02	4.65E+06 ± 1.0E+05
13-7-96-3	5.90E−01	2.425E+00 ± 9.44E−02	27.8	14.58 ± 0.06	4.53E+06 ± 1.8E+05
13-7-96-3	6.89E−01	2.604E+00 ± 1.02E−01	15.1	14.72 ± 0.04	4.86E+06 ± 1.9E+05
13-7-96-3	7.02E−01	2.591E+00 ± 1.06E−01	10.2	14.57 ± 0.04	4.84E+06 ± 2.0E+05
13-7-96-3	3.79E−01	2.649E+00 ± 1.60E−01	36.0	14.57 ± 0.05	4.95E+06 ± 3.0E+05
13-7-96-3	1.06E+00	2.433E+00 ± 3.89E−02	30.4	14.66 ± 0.05	4.55E+06 ± 7.3E+04

Table 2. (continued)

Sample	Mass, mg	$40^{*39}K$ 1σ	$^{40}Ar_{atm}$%	CA/K 1σ	Apparent Age 1σ
		6302B: J = 0.0010318 ± 0.000002035			
6302B	3.54E−01	1.983E+00 ± 1.16E−01	21.6	10.54 ± 0.04	3.69E+06 ± 2.2E+05
6302B	2.14E−01	2.012E+00 ± 1.62E−01	10.2	10.59 ± 0.06	3.74E+06 ± 3.0E+05
6302B	9.21E−01	1.886E+00 ± 5.97E−02	20.2	10.62 ± 0.03	3.51E+06 ± 1.1E+05
6302B	8.90E−01	1.907E+00 ± 4.81E−02	40.4	10.56 ± 0.03	3.55E+06 ± 9.0E+04
6302B	9.09E−01	1.829E+00 ± 5.76E−02	28.1	10.60 ± 0.04	3.40E+06 ± 1.1E+05
6302B	7.50E−01	1.886E+00 ± 6.66E−02	21.1	10.53 ± 0.02	3.51E+06 ± 1.2E+05
6302B	3.92E−01	1.609E+00 ± 8.36E−02	39.0	10.54 ± 0.04	2.99E+06 ± 1.6E+05
6302B	3.48E−01	1.561E+00 ± 1.14E−01	44.0	10.50 ± 0.06	2.90E+06 ± 2.1E+05
6302B	1.55E+00	1.731E+00 ± 2.66E−02	38.6	10.62 ± 0.02	3.22E+06 ± 5.0E+04
6302B	4.34E−01	1.502E+00 ± 4.35E−02	41.1	10.59 ± 0.04	2.79E+06 ± 8.1E+04
		DGR2: J = 0.00103666 ± 0.00000268			
DGR2	2.24E−01	1.564E+00 ± 3.45E−01	88.9	14.25 ± 0.09	2.92E+06 ± 6.4E+05
DGR2	1.20E+00	1.939E+00 ± 5.73E−02	73.5	11.62 ± 0.02	3.62E+06 ± 1.1E+05
DGR2	4.81E−01	1.778E+00 ± 1.53E−01	90.6	14.46 ± 0.04	3.32E+06 ± 2.9E+05
DGR2	3.08E−01	1.470E+00 ± 2.16E−01	91.3	14.13 ± 0.05	2.75E+06 ± 4.0E+05
DGR2	6.73E−01	1.968E+00 ± 1.37E−01	81.9	13.72 ± 0.05	3.68E+06 ± 2.6E+05
DGR2	9.01E−01	1.660E+00 ± 1.91E−01	89.6	16.75 ± 0.04	3.10E+06 ± 3.6E+05
DGR2	1.15E+00	1.782E+00 ± 9.89E−02	85.4	14.34 ± 0.03	3.33E+06 ± 1.8E+05
		DGR47: J = 0.00103666 ± 0.00000268			
DGR47	3.55E−01	1.786E+00 ± 1.45E−01	63.3	9.19 ± 0.03	3.34E+06 ± 2.7E+05
DGR47	1.42E+00	1.711E+00 ± 6.13E−02	76.2	10.30 ± 0.01	3.20E+06 ± 1.1E+05
DGR47	1.71E+00	1.838E+00 ± 6.03E−02	74.8	10.83 ± 0.01	3.43E+06 ± 1.1E+05
DGR47	9.03E−01	1.846E+00 ± 6.85E−02	73.3	9.49 ± 0.02	3.45E+06 ± 1.3E+05
DGR47	4.99E−01	1.976E+00 ± 1.43E−01	74.5	11.66 ± 0.03	3.69E+06 ± 2.7E+05
DGR47	7.07E−01	1.813E+00 ± 8.65E−02	74.3	8.62 ± 0.02	3.39E+06 ± 1.6E+05
		DGR9: J = 0.00103666 ± 0.00000268			
DGR9	6.55E−01	1.637E+00 ± 1.18E−01	71.2	19.39 ± 0.04	3.06E+06 ± 2.2E+05
DGR9	2.21E+00	1.751E+00 ± 2.03E−02	55.2	6.15 ± 0.01	3.27E+06 ± 3.9E+04
DGR9	1.55E+00	1.711E+00 ± 4.91E−02	75.4	10.70 ± 0.02	3.20E+06 ± 9.2E+04
DGR9	1.04E+00	1.764E+00 ± 6.10E−02	70.3	12.89 ± 0.02	3.30E+06 ± 1.1E+05
DGR9	8.48E−01	1.613E+00 ± 6.83E−02	76.0	11.85 ± 0.02	3.01E+06 ± 1.3E+05
DGR9	3.85E−01	1.923E+00 ± 1.21E−01	66.8	10.09 ± 0.03	3.59E+06 ± 2.3E+05
		K11: J = 0.00103666 ± 0.00000268			
K11	4.42E−01	1.889E+00 ± 1.37E−01	50.1	12.52 ± 0.04	3.53E+06 ± 2.5E+05
K11	1.55E+00	1.804E+00 ± 2.82E−02	62.1	13.92 ± 0.02	3.37E+06 ± 5.3E+04
K11	1.09E+00	1.779E+00 ± 4.54E−02	55.2	12.51 ± 0.02	3.32E+06 ± 8.5E+04
K11	7.16E−01	1.823E+00 ± 7.08E−02	62.4	14.28 ± 0.03	3.41E+06 ± 1.3E+05
K11	7.96E−01	1.797E+00 ± 5.89E−02	66.8	16.85 ± 0.03	3.36E+06 ± 1.1E+05
K11	6.91E−01	1.760E+00 ± 2.74E−02	64.4	11.91 ± 0.03	3.29E+06 ± 5.2E+04
K11	7.18E−01	1.916E+00 ± 7.00E−02	55.8	13.95 ± 0.04	3.58E+06 ± 1.3E+05
		K15: J = 0.00103666 ± 0.00000268			
K15	2.57E+00	1.710E+00 ± 1.93E−02	75.8	9.12 ± 0.01	3.20E+06 ± 3.7E+04
K15	1.22E+00	1.603E+00 ± 6.38E−02	83.2	8.24 ± 0.01	3.00E+06 ± 1.2E+05
K15	1.33E+00	1.692E+00 ± 2.27E−02	75.9	7.68 ± 0.01	3.16E+06 ± 4.3E+04
K15	4.46E−01	1.779E+00 ± 8.05E−02	83.3	8.01 ± 0.03	3.32E+06 ± 1.5E+05
K15	6.98E−01	1.886E+00 ± 5.88E−02	69.8	7.96 ± 0.02	3.52E+06 ± 1.1E+05
		K22: J = 0.00103666 ± 0.00000268			
K22	4.91E−01	2.002E+00 ± 2.08E−01	62.5	22.49 ± 0.10	3.74E+06 ± 3.9E+05
K22	8.08E−01	1.898E+00 ± 1.10E−01	70.9	22.53 ± 0.05	3.55E+06 ± 2.1E+05
K22	8.31E−01	1.923E+00 ± 1.81E−01	72.7	25.83 ± 0.08	3.59E+06 ± 3.4E+05
K22	4.12E−01	1.846E+00 ± 2.54E−01	70.8	21.42 ± 0.10	3.45E+06 ± 4.7E+05
K22	4.54E−01	2.129E+00 ± 2.20E−01	74.4	26.32 ± 0.08	3.98E+06 ± 4.1E+05
K22	1.94E−01	2.636E+00 ± 4.06E−01	56.8	21.18 ± 0.12	4.92E+06 ± 7.6E+05
K22	3.04E−01	2.018E+00 ± 2.33E−01	61.7	19.40 ± 0.09	3.77E+06 ± 4.3E+05
K22	3.53E−01	1.660E+00 ± 3.90E−01	77.1	26.63 ± 0.15	3.10E+06 ± 7.3E+05

Table 2. (continued)

Sample	Mass, mg	$40^{*39}K$ 1σ	$^{40}Ar_{atm}$%	CA/K 1σ	Apparent Age 1σ
K22	6.30E−01	1.856E+00 ± 1.65E−01	69.1	23.86 ± 0.06	3.47E+06 ± 3.1E+05
K22	5.40E−01	1.901E+00 ± 2.20E−01	72.8	22.86 ± 0.08	3.55E+06 ± 4.1E+05
		K31: J = 0.00103666 ± 0.00000268			
K31	1.79E+00	1.853E+00 ± 4.90E−02	65.8	10.45 ± 0.02	3.46E+06 ± 9.2E+04
K31	1.02E+00	1.935E+00 ± 5.33E−02	67.7	11.14 ± 0.02	3.61E+06 ± 1.0E+05
K31	7.44E−01	1.914E+00 ± 8.84E−02	71.6	10.96 ± 0.02	3.58E+06 ± 1.7E+05
K31	7.73E−01	2.047E+00 ± 6.49E−02	64.9	10.58 ± 0.02	3.82E+06 ± 1.2E+05
K31	8.37E−01	1.999E+00 ± 5.99E−02	65.3	10.15 ± 0.02	3.73E+06 ± 1.1E+05
		K38: J = 0.0010318 ± 0.000002035			
K38	1.94E−01	6.272E+00 ± 7.38E−01	64.8	22.28 ± 0.14	1.16E+07 ± 1.4E+06
K38	3.68E−01	7.266E+00 ± 9.15E−01	92.5	26.45 ± 0.10	1.35E+07 ± 1.7E+06
K38	2.38E−01	7.299E+00 ± 3.35E−01	38.3	15.69 ± 0.11	1.35E+07 ± 6.2E+05
K38	1.70E−01	7.299E+00 ± 3.19E−01	47.7	13.76 ± 0.12	1.35E+07 ± 5.9E+05
K38	5.40E−01	6.613E+00 ± 1.50E−01	67.4	19.98 ± 0.09	1.23E+07 ± 2.8E+05
K38	5.33E−01	6.810E+00 ± 2.19E−01	42.7	24.22 ± 0.10	1.26E+07 ± 4.0E+05
K38	4.53E−01	6.912E+00 ± 2.78E−01	75.2	21.38 ± 0.09	1.28E+07 ± 5.1E+05
K38	5.93E−01	6.602E+00 ± 2.54E−01	77.7	17.44 ± 0.10	1.22E+07 ± 4.7E+05
K38	6.95E−01	6.972E+00 ± 2.81E−01	88.5	20.35 ± 0.06	1.29E+07 ± 5.2E+05
K38	1.23E+00	6.646E+00 ± 2.19E−01	76.2	26.28 ± 0.07	1.23E+07 ± 4.1E+05
K38	9.31E−01	6.417E+00 ± 2.05E−01	70.8	17.13 ± 0.07	1.19E+07 ± 3.8E+05
		K43: J = 0.0010318 ± 0.000002035			
K43	5.61E−01	6.085E+00 ± 8.92E−02	37.5	8.14 ± 0.02	1.13E+07 ± 1.7E+05
K43	5.46E−01	5.960E+00 ± 6.79E−02	49.3	7.63 ± 0.03	1.11E+07 ± 1.3E+05
K43	5.01E−01	6.125E+00 ± 9.48E−02	35.9	7.98 ± 0.02	1.14E+07 ± 1.8E+05
K43	6.28E−01	5.959E+00 ± 6.59E−02	33.1	7.23 ± 0.02	1.11E+07 ± 1.2E+05
K43	6.62E−01	5.886E+00 ± 6.10E−02	41.4	8.04 ± 0.03	1.09E+07 ± 1.1E+05
K43	8.10E−01	5.914E+00 ± 4.25E−02	33.4	7.59 ± 0.02	1.10E+07 ± 8.2E+04
K43	1.01E+00	6.013E+00 ± 4.47E−02	37.2	7.34 ± 0.02	1.12E+07 ± 8.6E+04
K43	7.44E−01	5.930E+00 ± 7.20E−02	35.1	7.58 ± 0.02	1.10E+07 ± 1.3E+05
		K5: J = 0.00103666 ± 0.00000268			
K5	3.77E−01	2.102E+00 ± 3.87E−01	43.5	35.83 ± 0.17	3.93E+06 ± 7.2E+05
K5	4.90E−01	1.948E+00 ± 5.50E−01	53.1	51.60 ± 0.21	3.64E+06 ± 1.0E+06
K5	1.97E+00	1.818E+00 ± 5.95E−02	50.3	48.48 ± 0.17	3.40E+06 ± 1.1E+05
K5	7.68E−01	1.338E+00 ± 3.04E−01	71.9	46.62 ± 0.15	2.50E+06 ± 5.7E+05
K5	4.84E−01	2.245E+00 ± 4.37E−01	62.4	46.43 ± 0.17	4.19E+06 ± 8.2E+05
K5	3.13E−01	2.033E+00 ± 3.41E−01	76.2	33.71 ± 0.14	3.80E+06 ± 6.4E+05
K5	4.84E−01	1.412E+00 ± 2.08E−01	76.6	35.66 ± 0.14	2.64E+06 ± 3.9E+05
K5	1.13E+00	1.938E+00 ± 2.19E−01	49.2	46.37 ± 0.11	3.62E+06 ± 4.1E+05
K5	1.11E+00	1.720E+00 ± 1.97E−01	31.3	40.08 ± 0.10	3.21E+06 ± 3.7E+05
		MA152: J = 0.00103451 ± 0.00000196			
MA152	2.10E−01	1.385E+00 ± 3.25E−01	76.6	8.27 ± 0.04	2.58E+06 ± 6.0E+05
MA152	4.96E−01	1.317E+00 ± 7.96E−02	80.2	8.06 ± 0.01	2.46E+06 ± 1.5E+05
MA152	1.62E+00	1.418E+00 ± 4.41E−02	86.1	8.02 ± 0.01	2.65E+06 ± 8.2E+04
MA152	8.90E−01	1.311E+00 ± 4.79E−02	83.0	8.25 ± 0.02	2.45E+06 ± 8.9E+04
MA152	1.32E+00	1.524E+00 ± 5.75E−02	86.0	7.84 ± 0.01	2.84E+06 ± 1.1E+05
MA152	1.30E+00	1.405E+00 ± 3.21E−02	77.2	7.48 ± 0.02	2.62E+06 ± 6.0E+04
		MA170: J = 0.00103451 ± 0.00000196			
MA170	3.41E−01	1.849E+00 ± 1.13E−01	50.6	5.70 ± 0.02	3.45E+06 ± 2.1E+05
MA170	5.24E−01	1.903E+00 ± 9.78E−02	53.8	6.41 ± 0.02	3.55E+06 ± 1.8E+05
MA170	7.63E−01	1.795E+00 ± 6.43E−02	60.1	5.61 ± 0.01	3.35E+06 ± 1.2E+05
MA170	1.11E+00	1.791E+00 ± 4.43E−02	60.1	6.06 ± 0.01	3.34E+06 ± 8.3E+04
MA170	8.27E−01	1.880E+00 ± 5.34E−02	60.2	5.92 ± 0.01	3.50E+06 ± 1.0E+05
MA170	8.27E−01	1.853E+00 ± 5.27E−02	59.5	5.69 ± 0.01	3.46E+06 ± 9.8E+04
MA170	8.34E−01	1.686E+00 ± 3.94E−02	58.1	6.06 ± 0.01	3.14E+06 ± 7.4E+04
		MA203: J = 0.00103666 ± 0.00000268			

Table 2. (continued)

Sample	Mass, mg	$40^{*39}K$ 1σ	$^{40}Ar_{atm}$%	CA/K 1σ	Apparent Age 1σ
MA203	2.31E−01	4.540E+00 ± 1.37E+00	52.8	100.8 ± 1.24	8.47E+06 ± 2.6E+06
MA203	3.05E−01	2.452E+00 ± 1.30E+00	62.3	78.99 ± 0.48	4.58E+06 ± 2.4E+06
MA203	5.73E−01	1.766E+00 ± 2.63E−01	82.3	41.65 ± 0.13	3.30E+06 ± 4.9E+05
MA203	2.28E−01	2.369E+00 ± 9.86E−01	77.5	68.54 ± 0.54	4.42E+06 ± 1.8E+06
MA203	1.67E−01	9.529E−01 ± 1.40E+00	95.5	96.48 ± 0.67	1.78E+06 ± 2.6E+06
MA203	2.63E−01	1.273E−01 ± 1.15E+00	99.5	78.83 ± 0.59	2.38E+05 ± 2.1E+06
MA203	3.14E−01	2.353E+00 ± 9.53E−01	94.6	64.95 ± 0.34	4.39E+06 ± 1.8E+06
		MA208: J = 0.00103451 ± 0.00000196			
MA208	9.86E−01	2.202E+00 ± 4.14E−02	68.6	8.04 ± 0.02	4.10E+06 ± 7.7E+04
MA208	7.54E−01	2.179E+00 ± 6.32E−02	66.7	8.58 ± 0.02	4.06E+06 ± 1.2E+05
MA208	1.12E+00	2.167E+00 ± 3.75E−02	63.4	7.78 ± 0.02	4.04E+06 ± 7.0E+04
MA208	1.11E+00	2.218E+00 ± 3.49E−02	62.0	7.95 ± 0.02	4.13E+06 ± 6.5E+04
MA208	1.02E+00	2.223E+00 ± 4.45E−02	68.7	8.24 ± 0.01	4.14E+06 ± 8.3E+04
MA208	5.06E−01	2.139E+00 ± 1.11E−01	60.1	8.33 ± 0.05	3.99E+06 ± 2.1E+05
		MA227: J = 0.00103666 ± 0.00000268			
MA227	5.57E−01	1.943E+00 ± 1.18E−01	82.3	10.96 ± 0.02	3.63E+06 ± 2.2E+05
MA227	6.98E−01	2.170E+00 ± 9.79E−02	80.1	11.13 ± 0.03	4.05E+06 ± 1.8E+05
MA227	1.88E+00	1.987E+00 ± 8.47E−02	89.8	15.24 ± 0.03	3.71E+06 ± 1.6E+05
MA227	9.52E−01	2.107E+00 ± 6.99E−02	76.1	10.33 ± 0.02	3.94E+06 ± 1.3E+05
MA22	8.76E−01	2.147E+00 ± 5.48E−02	83.0	10.97 ± 0.02	4.01E+06 ± 1.0E+05
MA227	1.09E+00	2.086E+00 ± 5.45E−02	77.1	11.23 ± 0.02	3.90E+06 ± 1.0E+05
MA227	1.40E+00	2.093E+00 ± 4.02E−02	73.2	9.80 ± 0.02	3.91E+06 ± 7.6E+04
		MA37: J = 0.00103451 ± 0.00000196			
MA37	1.94E−01	1.114E+00 ± 2.11E−01	81.7	8.05 ± 0.03	2.08E+06 ± 3.9E+05
MA37	3.13E−01	9.513E−01 ± 1.17E−01	74.6	4.86 ± 0.02	1.77E+06 ± 2.2E+05
MA37	6.59E−01	6.512E−01 ± 6.26E−02	84.9	4.76 ± 0.01	1.22E+06 ± 1.2E+05
MA37	5.40E−01	7.069E−01 ± 7.78E−02	79.6	5.33 ± 0.01	1.32E+06 ± 1.5E+05
MA37	8.58E−01	7.349E−01 ± 3.21E−02	84.5	5.44 ± 0.02	1.37E+06 ± 6.0E+04
MA37	5.56E−01	9.555E−01 ± 7.96E−02	82.6	7.43 ± 0.02	1.78E+06 ± 1.5E+05
MA37	7.53E−01	8.678E−01 ± 5.46E−02	76.9	4.73 ± 0.01	1.62E+06 ± 1.0E+05
MA37	1.61E+00	7.258E−01 ± 2.35E−02	80.1	5.22 ± 0.01	1.35E+06 ± 4.4E+04
MA37	1.09E+00	6.834E−01 ± 4.83E−02	78.1	4.85 ± 0.01	1.28E+06 ± 9.0E+04
MA37	1.35E+00	8.075E−01 ± 2.74E−02	79.2	6.34 ± 0.01	1.51E+06 ± 5.1E+04
		MA85: J = 0.00103666 ± 0.00000268			
MA85	1.23E+00	8.129E−02 ± 3.37E−02	97.4	11.27 ± 0.02	1.52E+05 ± 6.3E+04
MA85	7.98E−01	9.311E−02 ± 4.60E−02	97.7	6.56 ± 0.01	1.74E+05 ± 8.6E+04
MA85	6.32E−01	2.128E−01 ± 8.38E−02	93.8	12.81 ± 0.03	3.98E+05 ± 1.6E+05
MA85	2.02E+00	5.032E−02 ± 3.33E−02	98.7	7.53 ± 0.01	9.41E+04 ± 6.2E+04
MA85	1.34E+00	7.004E−02 ± 5.39E−02	98.1	12.41 ± 0.02	1.31E+05 ± 1.0E+05
MA85	6.69E−01	4.286E−02 ± 5.62E−02	99.3	9.85 ± 0.02	8.02E+04 ± 1.1E+05
MA85	1.00E+00	2.007E−01 ± 3.32E−02	93.5	11.48 ± 0.04	3.75E+05 ± 6.2E+04
MA85	7.36E−01	1.352E−01 ± 4.79E−02	95.4	8.43 ± 0.02	2.53E+05 ± 9.0E+04
MA85	9.71E−01	4.905E−02 ± 3.87E−02	98.5	9.92 ± 0.02	9.17E+04 ± 7.2E+04
MA85	6.91E−01	4.714E−02 ± 7.62E−02	98.2	12.07 ± 0.03	8.82E+04 ± 1.4E+05
		MA75: J = 0.00103451 ± 0.00000196			
MA75	1.27E−01	1.564E+00 ± 3.59E−01	93.0	7.14 ± 0.05	2.92E+06 ± 6.7E+05
MA75	3.71E−01	9.997E−01 ± 1.90E−01	96.5	6.82 ± 0.02	1.86E+06 ± 3.6E+05
MA75	9.04E−01	1.274E+00 ± 1.28E−01	97.2	7.31 ± 0.02	2.38E+06 ± 2.4E+05
MA75	4.29E−01	6.829E−01 ± 1.77E−01	98.5	7.05 ± 0.03	1.27E+06 ± 3.3E+05
MA75	5.09E−01	7.332E−01 ± 2.47E−01	96.6	14.35 ± 0.07	1.37E+06 ± 4.6E+05
MA75	9.16E−01	8.749E−01 ± 8.30E−02	97.1	8.54 ± 0.02	1.63E+06 ± 1.5E+05

Table 3. Radiometric Ages Calculated From ^{40}Ar/^{39}Ar Isotope Composition of Whole Rocks, Plagioclase, and Amphibole Phenocrysts

Sample	*N*	Mean Apparent Age, Ma	MSWD	Isochron Age, Ma	MSWD (isochron)	Initial ^{40}AR/^{36}AR
			Madeira			
MA 85 (wr)	10	0.18 ± 0.08*	1.96	0.34 ± 0.34	1.77	286 ± 16
MA 19 (plag)	8	1.05 ± 0.16*	0.4	1.08 ± 0.22	0.44	288 ± 38
MA 82c (plag)	9	1.18 ± 0.10*	0.28	1.21 ± 0.28	0.31	293 ± 19
MA 146 (plag)	10	1.32 ± 0.30*	0.6	1.22 ± 0.82	0.66	300 ± 34
MA 37 (wr)	10	1.42 ± 0.08*	3.01	1.13 ± 0.56	2.92	309 ± 28
MA 107 (plag)	12	1.44 ± 0.06*	0.57	1.45 ± 0.12	0.67	295 ± 4
MA 75 (wr)	6	1.79 ± 0.36*	2.65	1.26 ± 1.60	3.05	297 ± 7
MA 152 (wr)	6	2.61 ± 0.10*	1.87	2.36 ± 0.38	1.74	301 ± 9
MA 44 (plag)	11	2.80 ± 0.06*	0.40	2.83 ± 0.08	0.37	295 ± 2
MA 170 (wr)	6	3.42 ± 0.10*	0.54	3.34 ± 1.20	0.67	298 ± 71
MA 227 (wr)	7	3.91 ± 0.08*	0.80	3.96 ± 0.24	0.89	294 ± 4
MA 208 (wr)	6	4.10 ± 0.06*	0.35	3.93 ± 0.52	0.36	300 ± 20
MA 203 (plag)	7	4.36 ± 0.40*	1.51	4.20 ± 0.62	1.45	292 ± 16
13-7-96-1 (glass)	7	4.48 ± 0.18*	1.19	4.47 ± 0.48	1.41	295 ± 6
13-7-96-3 (glass)	6	4.63 ± 0.10*	1.09	4.56 ± 0.32	1.38	295 ± 4
			Desertas Islands			
			Ilhéu Chão			
K 22 (wr)	10	3.62 ± 0.24*	0.55	3.43 ± 1.50	0.62	298 ± 50
			Deserta Grande			
DGR 9 (wr)	6	3.25 ± 0.08*	1.46	3.34 ± 0.20	1.80	289 ± 10
6302B (amph)	7	3.36 ± 0.12*	3.27	3.42 ± 0.52	3.83	279 ± 82
DGR 47 (wr)	6	3.38 ± 0.12*	0.89	3.14 ± 1.30	1.08	301 ± 40
DGR 2 (wr)	4	3.48 ± 0.18*	1.41	3.83 ± 0.36	0.60	288 ± 6
K 31 (wr)	5	3.62 ± 0.14*	1.72	3.14 ± 1.84	2.13	313 ± 74
			Ilhéu do Bugio			
K 15 (wr)	5	3.20 ± 0.94*	3.26	3.35 ± 0.68	3.95	290 ± 19
K 5 (plag)	9	3.36 ± 0.2*	1.08	3.19 ± 0.48	1.17	291 ± 31
K 11 (wr)	7	3.35 ± 0.06*	0.89	3.47 ± 0.44	0.86	286 ± 24
			Porto Santo			
K 43 (wr)	8	11.07 ± 0.10*	1.27	10.98 ± 0.46	1.52	298 ± 20
K 38 (plag)	11	12.50 ± 0.30*	1.14	12.35 ± 0.54	1.28	296 ± 4
K 67a (wr)	8	12.57 ± 0.12*	0.81	12.51 ± 0.26	0.84	296 ± 9
K 48 (wr)	6	15.40 ± 0.90	22.1	12.69 ± 0.82*	2.05	309 ± 4
K 47 (plag)	11	12.75 ± 0.26*	0.70	12.67 ± 0.46	0.80	294 ± 19
K 68 (wr)	7	12.90 ± 0.08*	0.80	12.05 ± 1.10	0.28	359 ± 82
K 42 (plag)	11	13.17 ± 0.58*	1.55	13.39 ± 1.06	1.74	291 ± 9
K 46 (plag)	10	13.59 ± 0.58*	1.37	13.56 ± 1.08	1.49	292 ± 12
K 55 (wr)	7	13.85 ± 0.34*	2.90	12.90 ± 4.10	3.37	302 ± 30
K 49 (plag)	11	14.31 ± 0.22*	1.0	14.45 ± 0.32	0.88	291 ± 4
			Ampére Seamount			
DS 797-1 (wr)	13	31.20 ± 0.20*	1.33	32.70 ± 0.92	0.69	285 ± 6

*Accepted ages.

N, number of single crystals/whole rock particles fused. Errors are quoted at the 2σ level. MSWD, mean square weighted deviates; wr, whole rock; plag, plagioclase; amph, amphibole phenocrysts.

an age of 3.42 ± 0.10 Ma, was taken from a lava flow at Machico near the easternmost tip of Madeira, where Madeira joins the Desertas submarine ridge (see Figure 2).

[21] Samples from the middle unit range in age from 1.0 to 2.8 Ma. At Paul da Serra (Figure 5), the middle unit fills in a paleocanyon in the basal unit, reaching a thickness of up to 500 m. Plagioclase crystals (MA 44) from a pumice layer, just above

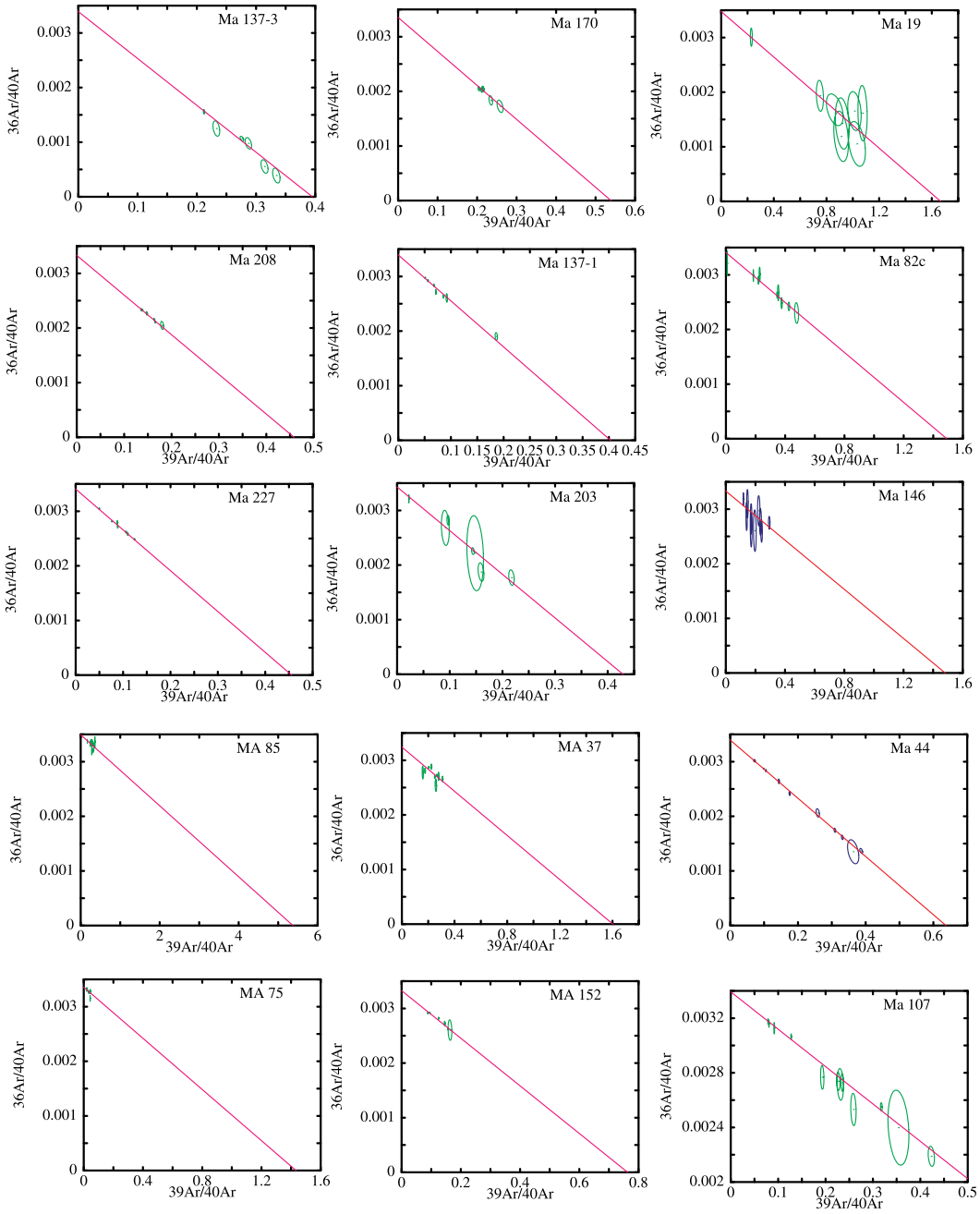

Figure 6. Isotope correlation diagrams for Ar isotope compositions of fused plagioclase phenocrysts, glass, and whole rock samples of Madeira.

this unconformity on the paleohill forming part of the southern wall of the canyon, yielded an age of 2.80 ± 0.06 Ma. The unconformity separates this pumice layer from basal unit samples MA 208 and MA 203 with ages of 4.10 ± 0.06 and 4.36 ± 0.40 Ma sampled about 300 m below the unconformity at the same locality. A lava flow (MA 37) and pumice layer (MA 19), stratigraphically overlying the 2.8 Myr old pumice layer, were dated at 1.42 ± 0.08 and 1.05 ± 0.16 Ma, respectively. Additional samples from the middle unit (MA 75, MA 152, MA 146, and MA 107) fall within the range found at Paul da Serra (1.0–2.8 Ma). In the southeastern part of the island (at the coast halfway between Funchal and Machico), *Watkins and Abdel-Monem* [1971] report K/Ar ages between 1.76 Ma at the base and 0.74 Ma at the top of a road profile (Figure 3). Plagioclase crystals (MA 107) from a pumice layer between the second (1.64 Ma) and the third (1.05 Ma) lowest flow produced an

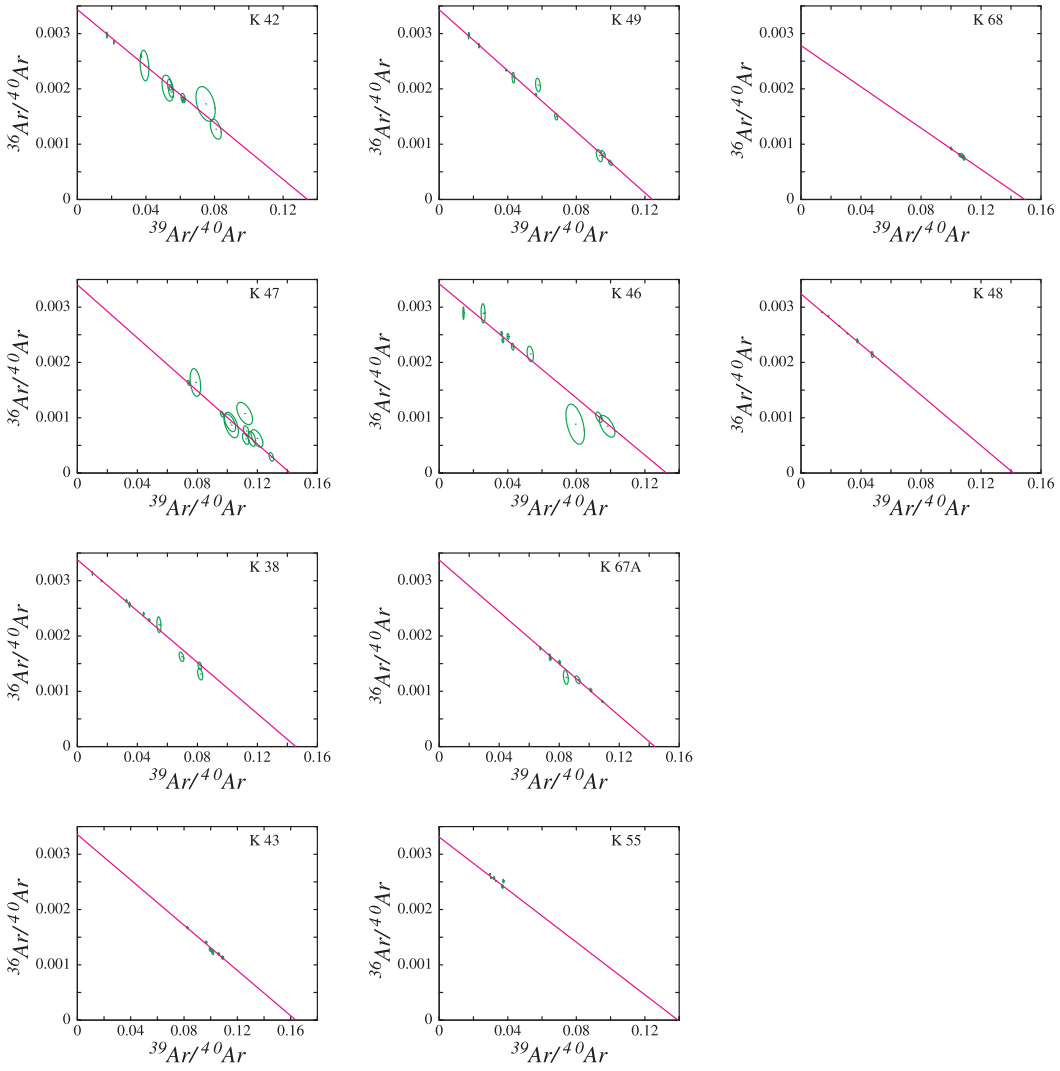

Figure 7. Isotope correlation diagrams for Ar isotope compositions of fused plagioclase phenocryst and whole rock samples from Porto Santo.

^{40}Ar/^{39}Ar age of 1.44 ± 0.06 Ma, in good agreement with the K/Ar ages of *Watkins and Abdel-Monem* [1971].

[22] The upper unit on Madeira consists of numerous cinder cones and intracanyon lava flows, for example, at Porto do Moniz, Seixal, and São Vicente (Figure 3). Sample MA 85 from the pahoehoe lava sequence at São Vicente, which originates from the top of Paul da Serra, yields a young age of 0.18 ± 0.08 Ma. Two charcoal samples were collected beneath a tephra layer on top of Paul da Serra. The samples have calibrated ^{14}C ages of 6407–6496 years B.P. (KIA 685) and 7159–7216 years B.P. (KIA 686), confirming a Holocene age of ~6450 years B.P., as previously mentioned by *Schmincke* [1998].

4.2. Desertas Islands (Ilhéu Chão, Deserta Grande, and Ilhéu do Bugio)

[23] All nine rocks dated from the Desertas Islands fall within a narrow range of 3.2–3.6 Ma (Figure 3). A profile through the entire stratigraphic column exposed on Deserta Grande is shown in Figure 4. The oldest ages come from the lava flows at the base of the lava succession on Deserta Grande and Ilhéu Chão with 3.62 ± 0.14 (K 31), 3.48 ± 0.18 Ma (DGR 2), and 3.62 ± 0.24 (K 22), respectively. Samples from a lava flow (DGR 47) and from an amphibole megacryst in a scoria cone from the top of Deserta Grande yielded identical ages within error of 3.38 ± 0.12 and 3.36 ± 0.12, respectively. A young dike (DGR 9) that cuts the entire lava pile gives a similar age of 3.25 ± 0.08 Ma. A basaltic beach cobble from the western

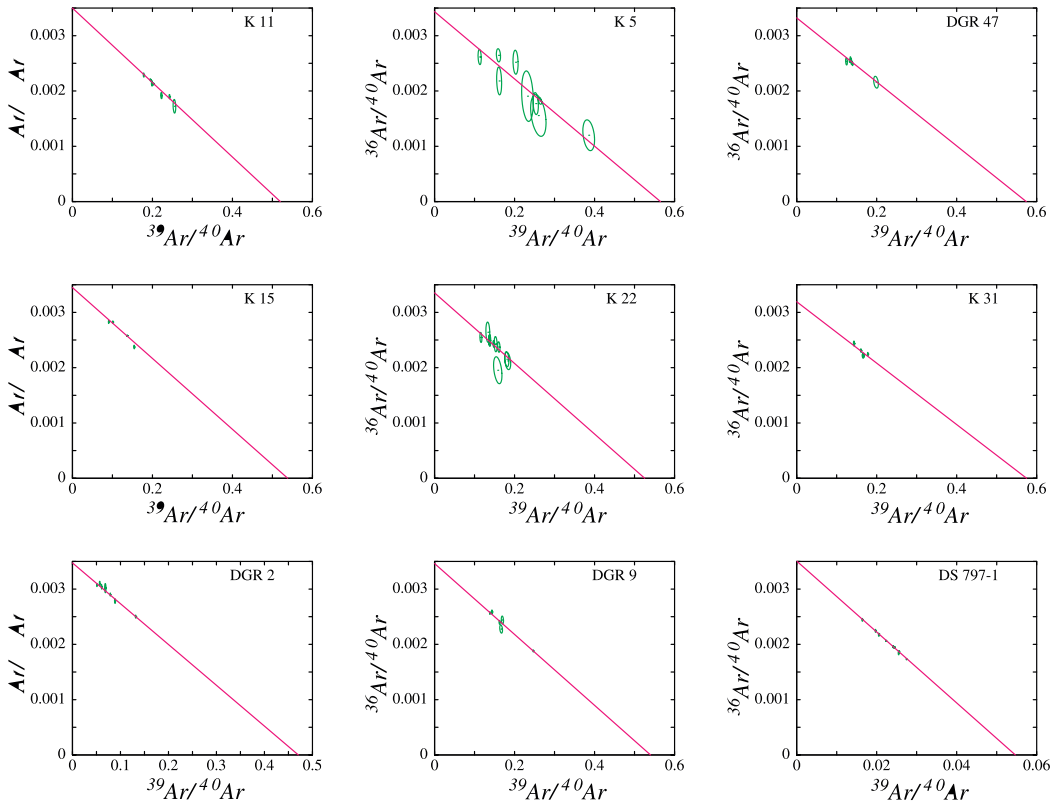

Figure 8. Isotope correlation diagrams for Ar isotope compositions of fused whole rock and plagioclase phenocryst samples from the Desertas Islands and Ampère Seamount.

shore of Ilhéu do Bugio produced an age of 3.35 ± 0.06 Ma (K 11); dikes from the same island which cut the entire lava sequence give ages of 3.35 ± 0.06 and 3.36 ± 0.2 Ma (K5, K15), within error of the youngest units from Deserta Grande.

4.3. Porto Santo

[24] Samples from Porto Santo have older ages (11.1–14.3 Ma) than found on Madeira or the Desertas Islands (Table 3, Figure 3). The investigated samples cover the entire stratigraphic succession of the island: clastic seamount stage in the NE, alkali basaltic lava sequence in the SW, and dikes and minor trachytic and basaltic intrusions which cut both units. The oldest age (14.31 ± 0.22 Ma) comes from a benmoreitic dike (K 49) associated with a trachytic intrusion belonging to the seamount stage in the northwest part of the island. Sample K 55 from a submarine lava flow with an age of 13.85 ± 0.34 Ma comes from the base of the basaltic to hawaiitic sequence of lava flows at the southwestern end of the island. Dikes and intrusions of both mafic and evolved composition (K 38, K 42, K 47, K 67a, K 68) from the NE and SW of the island yield ages between 12.5 and 13.2 Ma (see Table 3). The youngest age from Porto Santo (11.07 ± 0.10 Ma) comes from a basanitic intrusion (K 43).

4.4. Ampère Seamount

[25] A rounded beach cobble of hawaiitic composition (DS 797-1) from Ampère Seamount gives the oldest age (31.2 ± 0.2 Ma) of the samples dated in this study. This sample was dredged from the

Table 4. Radiocarbon Ages of Charcoal

Sample	Conventional Age, years B.P.	Corrected FMC	$\delta^{13}C$, ‰	Calibrated Age,* years B.P.
KIA 685	5670 ± 60	0.4936 ± 0.0038	−20.49 ± 0.26	6407–6496
KIA 686	6270 ± 60	0.4584 ± 0.0033	−19.50 ± 0.20	7159–7216

* Translation into calibrated age according to *Stuiver and Reimer*[1993]. Ages referred to before present (1950). Errors at 1σ level.

eastern part of the summit plateau of Ampère in 160 m water depth (see Table 1).

5. Discussion

5.1. Geochronological Evolution of Madeira and the Desertas Islands

[26] Considering the new $^{40}Ar/^{39}Ar$ age determinations and field observations, the old stratigraphic division based on the lithological mapping by *Zbyszewski et al.* [1973, 1975] has to be partly revised. We propose the following evolution for Madeira.

5.1.1. Shield Stage (>4.6–0.7 Ma)

5.1.1.1. Early Madeira Rift Phase (>4.6–3.9 Ma)

[27] This volcanic phase includes the oldest subaerial exposed rocks of Madeira (basal unit). A concentration of volcanic vents and east-west oriented dike swarms in the center of the eastern half of the island suggest that volcanism during the early Madeira rift phase primarily originated from an E–W orientated rift system. The oldest radiometric ages (4.63 ± 0.10 Ma) from Madeira come from an east-west oriented tholeiitic dike swarm at Porto da Cruz. Rift zones are a common feature of oceanic volcanic islands [e.g., *Carracedo*, 1994]. In the ideal case, triple-armed rift zones with regular geometry at 120° to one another occur as a result of least effort fracturing produced by magma-induced vertical upward loading [*Luongo et al.*, 1991]. As is the case with many Hawaiian volcanoes (e.g., Kilauea), a third rift zone on Madeira with an angle at about 120° to both other arms could probably not develop to the NE because of the buttressing effect of the large submarine cone of Porto Santo Island (Figure 2).

5.1.1.2. Desertas Rift Phase (3.6–3.2 Ma)

[28] The subaerial part of the Desertas Ridge formed between 3.2 and 3.6 Ma, during which time Madeira was almost completely inactive. At the Paul da Serra profile in central Madeira, an unconformity marks this time interval (Figure 4). In eastern Madeira north of Funchal, an unconformity also occurs separating the early and late Madeira rift phases. The lowermost flow of the late rift phase, just above the unconformity, was dated at 3.05 Ma [*Watkins and Abdel-Monem*, 1971]. No age data are available from rocks beneath the unconformity. A lava flow just above a prominent unconformity with the early Madeira rift phase (basal unit) in Curral das Freiras produced an age of 2.97 Ma [*Mata et al.*, 1995]. The youngest age from below the unconformity is 3.91 ± 0.08 Ma (MA 227). These observations suggest that most of the magma supply shifted to the Desertas rift arm between 3.0 and 3.9 Ma. Although speculative, one possible cause for the shift in magma supply between 3.9 and 3.6 Ma to the Desertas rift arm may have been collapse of the NE sector of the Madeira Rift Arm (see Figure 2). The bathymetry north of Porto da Cruz is very irregular at depths between 1000 and 2000 m, possibly reflecting the presence of landslide deposits. More detailed bathymetry, however, is necessary to test this hypothesis. A similar scenario has been proposed for the shift of volcanic activity on La Palma (Canary Islands) to the N–S oriented La Cumbre Vieja rift from the Taburiente shield volcano 700,000 years ago [*Ancochea et al.*, 1994; *Klügel et al.*, 2000]. At around 3 Ma, volcanism along the Desertas Rift arm ceased, possibly reflecting a shift in the magma supply further to the SW as a result of NE directed plate motion.

5.1.1.3. Late Madeira Rift Phase (3–0.7 Ma)

[29] Beginning at ~3 Ma, volcanic activity shifted back to Madeira. As noted above, at Paul da Serra, Curral das Freiras and Ribeiro Frio, the oldest flows overlying major unconformities separating the early and late Madeira rift phase yielded ages between 2.8 and 3.0 Ma [*Watkins and Abdel-Monem*, 1971; *Mata et al.*, 1995; this study]. Field observations and age dates from thick lava sequences that cover most of the island show that the late Madeira rift phase continued without a significant pause until 0.7 Ma. Although previously mapped as belonging to the basal unit (β1 of *Zbyszewski et al.* [1975]), scoria cone complexes such as Pico Ruivo (2.6 Ma), the highest peak on Madeira, and those near the São Lourenço peninsula (1.6–1.9 Ma [*Mata et al.*, 1995]) yield ages within the range for the late rift stage. These eruption centers are located along the axis of the late Madeira rift and are cut by dense dike swarms oriented in the E–W direction. Four of these dikes near Pico Ruivo yield ages between 1–1.8 Ma [*Féraud et al.*, 1981], showing that they are contemporaneous with the thick lava sequences dipping gently to the north and south and thus probably represent feeder dikes for the late Madeira rift phase lava sequences.

5.1.2. Posterosional Stage (<0.7 Ma)

[30] Because of the uncertainties in radiometric age dating of young magmatic rocks, the exact gap between the end of the Madeira rift phase and the posterosional stage is uncertain. The two deposits from this stage that have been dated thus far yield ages of ~0.2 Ma (MA 85) and 6200–7200 years B.P. (KIA 685 and KIA 686). It is conspicuous that the youngest activity (e.g., cinder cones in upper São Vicente valley, intracanyon flows at Porto do Moniz, Seixal, São Vicente, and the tephra layer on top of Paul da Serra) are located in the western part of Madeira, whereas the oldest rocks are found in the eastern part and the center of the island. The generally westward migration of volcanism on Madeira could potentially reflect NE motion of the African Plate.

5.2. Eruption Rates

[31] Estimating the subaerial volume of Madeira (~430 km^3) and the Desertas Islands (~7 km^3) and considering the oldest available radiometric age (4.63 Ma), an average magma eruption rate of ~95 km^3/Ma can be calculated for the subearial part of the shield stage. Upon closer examination of eruption rates for the different units, distinct differences become apparent. Whereas the early Madeira rift phase shows relatively high rates of 150 km^3/Ma, magma eruption decreased during the Desertas rift phase to 20 km3/Ma and increased again to 100 km^3/Ma during the late Madeira rift phase. Although erosion may have removed a considerable volume from the Desertas, it is unlikely that eruption rates during the subaerial Desertas rift phase approached those of the Madeira rift phases. As has been suggested to explain the shift of activity to the Desertas Rift, the decrease in eruption rates between ~3.0 and 3.9 Ma could also result from blocking of the magma plumbing system due to sector collapse. This may have caused an increase in intrusion relative to extrusion during the Desertas rift phase. The eruption rate during the posterosional stage of ~2 km^3/Ma is negligible.

[32] The hotspots with the lowest estimated eruption rates occur in the Atlantic Ocean. These include St. Helena (24 km^3/Ma), Bouvet (40 km^3/Ma), Cape Verdes (40 km^3/Ma), Ascension (60 km^3/Ma), and Gough (110 km^3/Ma) [*Gerlach*, 1990; see also *Crisp*, 1984; *Bohrson et al.*, 1996]. The eruption rates reported for these islands fall within the range determined for Madeira: 20–150 km^3/Ma. It should be noted, however, that it is difficult to directly compare eruption rates for individual islands, since these estimates are often averages for the entire island and often it has not been determined which evolutionary stage(s) the island was in during its subaerial history. Eruption rates for Madeira, on the other hand, are considerably lower than those estimated for the Canary Islands (e.g., 2000–10,000 km^3/Ma for the subaerial Miocene shield stage and up to 500 km^3/Ma for the posterosional stage on Gran Canaria [*Bogaard et al.*, 1988; *Hoernle and Schmincke*, 1993a; *Schmincke and Sumita*, 1998]). Madeira also shows low (subaerial) eruption rates when compared to ocean islands in the Indian and Pacific Oceans, for example, Reunion (2400 km^3/Ma) or Mangaia (100–1000 km^3/Ma) [*Gerlach*, 1990].

[33] The submarine base of the Madeira/Desertas group makes up ~98% of the volcanic complex, having a volume of ~26,800 km^3. The submarine volumes were estimated on the basis of the break in the bathymetry between the volcanic edifice and the gentle seafloor. Calculating an eruption rate for the submarine base is difficult owing to lack of age data and speculative assessment of the intrusive to extrusive ratio. We realize that the volume at the edifice hidden in the clastic apron may be 2–3 times more than the estimate based on the bathymetry alone, as seen, e.g., for Gran Canaria [*Schmincke and Sumita*, 1998]. Assuming that the Madeira/Desertas complex began forming ~9.5 Myr ago (an age intermediate between the oldest ages obtained from Madeira and Porto Santo), the average rate of growth during the submarine stage was ~5500 km^3/Ma or ~36 times as high as during the early subaerial rift stage on Madeira. However, in comparison to other ocean island volcanoes, Madeira has a relatively low average submarine growth rate. Production rates of >20,000 km^3/Ma have been estimated for the nearby Canary Islands [*Schmincke and Sumita*, 1998].

5.3. Geochronological Evolution of Porto Santo (11.1–14.3 Ma)

[34] The $^{40}Ar/^{39}Ar$ age data (samples K 49 and K 46) from the trachytic to basaltic submarine sequence in the northeast are in good agreement with paleontological data from intercalated shallow water limestones [*Cachao et al.*, 1998]. Both types of data yield an age of ~14 Ma for the end of the seamount stage in NE Porto Santo. An alkali basaltic lava flow (K 55) overlying pillow basalts but underlying a conglomerate consisting of beach

cobbles and boulders produced a similar age, indicating that the transition from seamount to ocean island in the SW also occurred at ~14 Ma. Seven samples from basaltic and trachytic dikes and intrusions ranged in age from 11.07 to 13.17 Ma, probably reflecting the time span of active volcanism on Porto Santo. Most of this subaerial history, however, has been eroded away.

5.4. Seine, Ampère (31 Ma), and Coral Patch Seamount

[35] Bathymetric data show that Seine and Ampère Seamounts have flat summit plateaus between 60 and 200 m below sea level and steep flanks. The morphology of both seamounts and the occurrence of well-rounded beach cobbles among dredged samples from Ampère Seamount indicate that both were probably islands formerly. A highly vesicular scoria sample, dredged from the 1000 m deep summit of nearby Coral Patch Seamount, also points to a shallow water or possible subaerial origin. Ocean island volcanoes that form above a hotspot are generally drowned as the volcano moves away from the hotspot as a result of (1) cessation of magma supply, (2) erosion, and (3) cooling and subsidence of the underlying lithosphere [e.g., *Werner et al.*, 1999]. The E–W elongated shape of the Ampère/Coral Patch structure may be related to old fracture zones in the oceanic crust which were used by the rising magma.

5.5. The Madeira Hotspot Track

[36] Considering the assumed NE directed African plate motion [e.g., *Duncan*, 1981; *Morgan*, 1983] and the available geochemical (J. Geldmacher and K. Hoernle, manuscript in preparation, 2000), age, and bathymetric data for the entire region, a specific Madeira hotspot track can be proposed (Figure 1). The hotspot track includes the Madeira/Desertas volcanic complex, Porto Santo Island, Seine Seamount, possibly Unicorn Seamount, Ampère Seamount, Coral Patch Seamount, and the upper alkaline summit of Ormonde Seamount. The presence of alkaline rocks on Ormonde Seamount is consistent with a hotspot origin. The $^{40}Ar/^{39}Ar$ age dating of these rocks (65–67 Ma [Féraud et al., 1982, 1986]) further shows that they are significantly younger than the underlying early Cretaceous oceanic lithosphere. For these reasons, we believe that the alkaline top of Ormond Seamount could be part of the Madeira hotspot track.

[37] As the distance from Madeira/Desertas (0 to >4.6 Ma) increases, the age of volcanic and plutonic rocks becomes systematically older: Porto Santo (11–14.3 Ma), Ampère (31 Ma), Ormonde (65–67 Ma). A small seamount off the SW coast of Madeira (Figure 2) extending from ~4000 m water depths up to 500 m below sea level is assumed to mark the present center/surface expression of the Madeira hotspot.

[38] In order to determine the rate of plate motion for the underlying plate from a hotspot track, the oldest ages from each volcano are generally used, assuming that they are similar to the ages of the main stage of volcanism when the volcano lay over the center of the hotspot. We note, however, that on a slow plate, such as the NW part of the African Plate, there may be several million years difference in the oldest age obtained from samples on the top and on the flanks of an island/seamount and the main growth stage, resulting in larger errors for the plate motion. On Madeira, for example, fossils from reef debris of "Vindobonian" age, which corresponds to an age between 5.2 and 6 Ma [*Carvalho and Brandão*, 1991; *Schmincke*, 1998], occur in uplifted parts of the submarine base of the island.

[39] As illustrated in Figure 9, age relationship of the volcanoes (using the oldest available radiometric ages from each volcano) against distance from Madeira shows a linear correlation. The slope of the correlation line yields a calculated absolute plate velocity of 1.2 cm/yr above the Madeira hotspot (with the condition that the hotspot is fixed in respect to the overriding plate). From Seine Seamount, located midway between Porto Santo and Ampère Seamount, no age data are available, but regarding the position on the correlation line in Figure 9 an age of 25–30 Ma is predicted.

[40] The Madeira hotspot track can be traced beyond Ormonde Seamount to the other side of the Azores-Gibraltar fracture zone as proposed by *Morgan* [1983]. Taking right lateral strike-slip motion between 60 and 72 Ma along the Azores-Gibraltar fracture zone into consideration [*Purdy*, 1975], the 70–72 Myr old [*McIntyre and Berger*, 1982] alkaline Serra de Monchique complex in southern Portugal could represent the continuation of the Madeira hotspot track on the Eurasian plate (Figure 1). The lateral distance between Ormonde Seamount and Serra de Monchique of ~270 km agree well with the ~200 km wide offset of the magnetic anomalies 31–34 across the Azores-Gibraltar fracture zone [*Cande and Kristoffersen*, 1977]. The close relationship is also supported by the proposed geochemical similarities between the

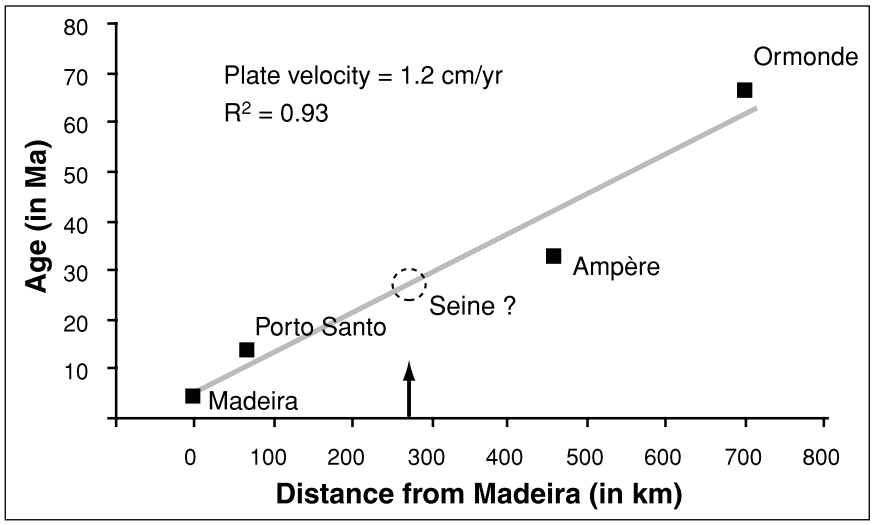

Figure 9. Age (oldest available from each volcano; see text for details) versus distance from Madeira (midpoint of each volcano). From Seine Seamount no age data are available, but considering the distance from Madeira, an age of 25–30 Ma is predicted.

Serra de Monchique and Ormond magmatic rocks [*Bernard-Griffiths et al.*, 1997].

[41] On the basis of the curvature of the proposed Madeira hotspot track, the rotation pole for the African Plate has been modeled by calculating the intersections of big circles placed orthogonal to the track (Figure 10). Assuming an ideal case, the centers of Madeira (32°45′/ 17°00′), Porto Santo (33°03′/16°20), Ampère Seamount (35°04/12°56′), and Ormonde Seamount (36°42/11°08′9) were selected as fixed points for the track. The calculated pole at 43°36′N/24°33′W correlates well with the rotation pole calculated by *Duncan* [1981] at 38°N/30°W for the time period of 0–55 Ma (Figure 10), using the South Atlantic hotspot tracks. *Pollitz* [1991] propose a change in the location of the pole at ~6 Ma to a position at 18.5°N/15.8°W, and therefore only the rotation polefor the 6–30 Ma time interval is shown. The 6–30 Ma pole does not fit the proposed Madeira hotspot track and also cannot explain the spatial distribution of the Canary Islands. The postulated pole change at 6 Ma is not evident in the Madeira hotspot system because it would require a shift in the volcanic age progression to the east (which would probably have resulted in reactivation of Porto Santo volcano).

[42] On the basis of the position of islands and seamounts an angular velocity of 0.47°/Ma can be calculated, which converts into an absolute plate motion of 1.2 ± 0.7 cm/yr above the Madeira hotspot. The large error range results from (1) the short overall length of the Madeira hotspot track due to the proximity to the rotation pole and (2) uncertainty in integrating over a long time period in which possible variations in plate velocity or pole position are averaged. For example, *O'Conner et al.* [1999] proposed a decrease in African Plate velocity since 19–30 Ma. The Madeira hotspot track differs from most other hotspot tracks in two important ways: (1) The track is irregularly distributed (e.g., elongated alignment of Ampère and Coral Patch Seamounts (EW) and possibly Seine and Unicorn (N–S)). (2) There are large and varying distances between individual volcanic complexes. Both of these features, in addition to the very low eruption/production rates, could be explained by a weak, pulsating or blob-type plume, as has been proposed for the Canary Islands [*Hoernle and Schmincke*, 1993b]. Assuming that mantle upwelling is in the form of discrete spherical blobs, as has been observed in numerical models for plume initiation [e.g., *Keken*, 1997], their ascent rate will be proportional to the square of the radius of the blob (Stokes' law). This means that small blobs rise very slowly and are more susceptible to displacement during ascent owing to the more horizontal asthenospheric mantle flow than larger ones, which have a higher ascent rate, resulting in irregularly distributed volcanoes at the surface. The large age differences and distances between large volcanoes and volcanic complexes along the hotspot track suggest that intervals of up to 10–25 Ma may separate individual pulses (or blobs) of upwelling plume mantle.

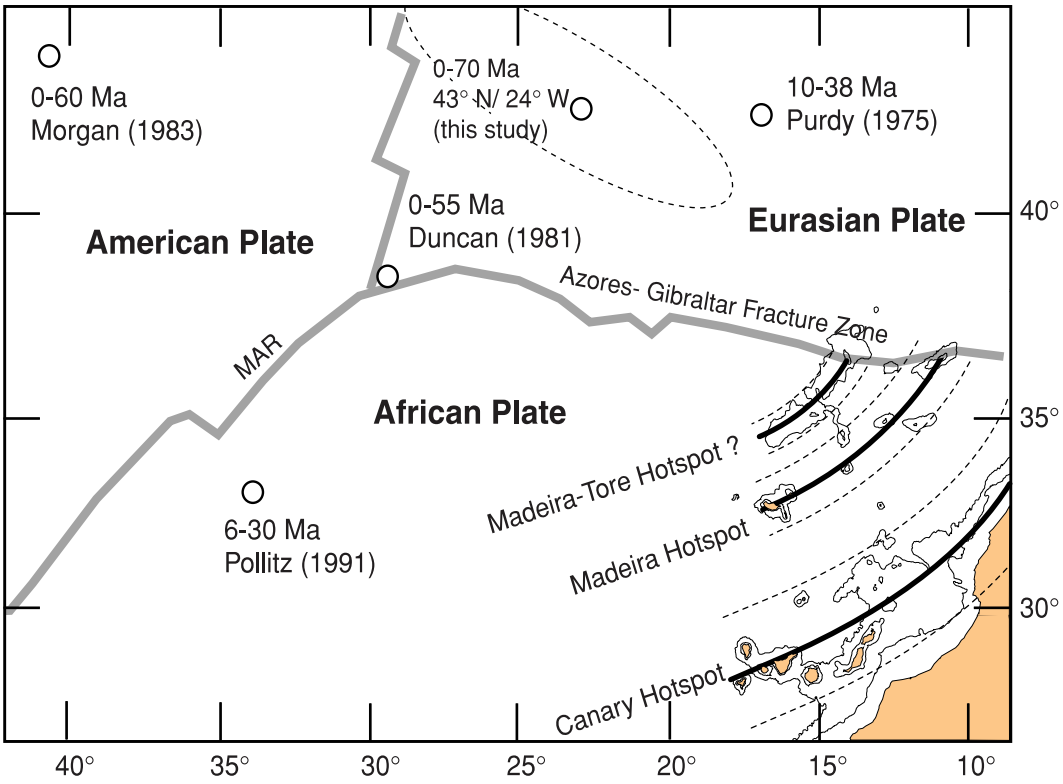

Figure 10. Location of rotation pole for the African Plate (valid for the time period 0–70 Ma) based on the proposed Madeira hotspot track. The African Plate motion is a counterclockwise rotation about a pole at 43°N/24°W. An error ellipse was calculated for this pole by calculating the intersections of big circles placed orthogonal to the outer limits of the track. For comparison, rotation poles of *Purdy* [1975], *Duncan* [1981], *Morgan* [1983], and *Pollitz* [1991] for the periods of 10–38 Ma, 0–55 Ma, 0–60 Ma, and 6–30 Ma, respectively, are also shown. Possible hotspot tracks are also indicated for the Canary Islands and the Madeira-Tore Rise.

[43] The elongation of the Madeira-Tore Rise (Figure 1) does not point to Madeira but rather to the west of Madeira. On the basis of gravimetric data it has been proposed that the Madeira-Tore Rise was formed at the Mid-Atlantic Ridge [*Peirce and Barton*, 1991]. However, samples from the top of Josephine Seamount, at the NE end of the Madeira-Tore Rise, have alkali basaltic compositions and Miocene ages [*Eckhardt et al.*, 1975; *Wendt et al.*, 1976; *Matveyenkov et al.*, 1994]. This could be explained by production of minor volcanism associated with the movement along the Azores-Gibraltar fracture zone. *Wendt et al.* [1976] note the coincidence of eruption age and intensive convergence tectonics and uplift along this boundary. Alternatively, the Madeira-Tore Rise could be interpreted as a separate hotspot track, formed by a separate small hotspot north or west of Madeira (see Figure 10). This would be consistent with the available geochemical data from Josephine Seamount. Additional age and geochemical data from seamounts forming the Madeira-Tore Rise, however, are necessary to test this hypothesis.

[44] Using the calculated Euler Pole for the proposed Madeira hotspot track, the Selvagen Islands and the seamounts southeast of Madeira and northeast of the Canary Islands could belong to the earlier part of the nearby Canary Island hotspot track (Figure 10). This has also been proposed on the basis of geophysical [*Holik and Rabinowitz*, 1991], geochemical, and geochronological (J. Geldmacher et al., manuscript in preparation, 2000) studies. If these seamounts and the Selvagen and Canary Islands result from a single hotspot, this plume must be considerably wider (~400 km) than the proposed Madeira or possible Madeira-Tore Rise plumes (~150–200 km).

6. Conclusions

[45] Madeira and the Desertas Islands form a single volcanic system consisting of the E–W oriented Madeira rift arm and the NNW–SSE Desertas rift arm. The two rift arms join at the eastern end of Madeira and northern end of the 60 km long, primarily submarine Desertas Ridge at an angle

of 110°. The subaerial evolution of the Madeira/Desertas volcanic system can be divided into a voluminous (99.5% of the subaerial volume) shield stage (>4.6–0.7 Ma) and a low-volume (0.5%) posterosional stage (<0.7 Ma). During the shield stage, volcanism occurred on Madeira almost exclusively from 3.9 to 4.6 Ma (early Madeira rift phase) and from 0.7 to 3.0 Ma (late Madeira rift phase). The Desertas Islands formed in a short interval between 3.2 and 3.6 Ma, during which time the Madeira Rift was almost completely inactive, possibly reflecting blockage of the central and western parts of the Madeira rift arm due to collapse of the NE sector of the Madeira Rift. Minor posterosional volcanism continued into the Holocene with the last eruption on Madeira occurring 6000–7000 years B.P. Average growth rates for the submarine (5500 km^3/Ma) and subaerial (100–150 km^3/Ma) shield stages on Madeira are among the lowest found for ocean island volcanoes.

[46] A shallow seamount SW of Madeira probably marks the present location of the >70 Myr old Madeira hotspot track, which includes the Madeira/Desertas volcanic system (0–4.6 Ma), Porto Santo Island (11.1–14.3 Ma), Seine, possibly Unicorn, Ampère (31 Ma), Coral Patch, and Ormonde (65–67 Ma) Seamounts, and the Serra de Monchique intrusive complex (70–72 Ma) in southern Portugal. On the basis of the proposed Madeira hotspot track, we calculate a rotation pole at 43°36′N/24°33′W and an angular velocity of 0.47°/Ma for the African Plate with a plate motion above the Madeira hotspot of 1.2 cm/yr, which agrees well with the pole of rotation for the African Plate calculated by *Duncan* [1981] using the South Atlantic hotspot tracks. The large and varible age gaps between individual volcanoes in the Madeira hotspot track, in addition to the very low magmatic productivity, can best be explained by a very weak hotspot, which is only intermittently active.

Acknowledgment

[47] We thank Director H. Costa-Neves and the staff from the Parque Natural da Madeira for cooperation and excellent logistical support during field studies on Madeira and especially the Desertas Islands. Captain M. Gross, officers, and crew of the F.S. *Poseidon* are gratefully acknowledged for their help in obtaining submarine rock samples used in this study. Especial thanks to R. Schmidt and A. Klügel for stimulating discussions in and out of the field. G. Zankl and F. Marks assisted with sample preparation. J. Sticklus provided technical support during $^{40}Ar/^{39}Ar$ laser dating at Geomar. Many thanks also to D. Rodriguez (University of Madeira) and H. Blazy (University Hamburg) for varied help. S. Karstel (Geomar) is thanked for providing bathymetric maps. We thank H. Staudigel, Sinton, M. Reid, and W. White for their constructive reviews, which have led to significant improvements. This study was supported by Deutsche Forschungsgemeinschaft project Ho 1833/1.

References

Ancochea, A., F. Hernén, A. Cendrero, J.M. Cantagrel, J.M. Fúster, E. Ibarolla, and J. Coello (1994), Constructive and destructive episodes in the building of a young oceanic island, La Palma, Canary Islands, and genesis of the Caldera de Taburiente, *J. Volcanol. Geotherm. Res.*, *60*, 243–262.

Auzende, J. M., J. Olivet, A.Le Lann, X.Le Pichon, J. Monteiro, A. Nicolas, and A. Ribeiro (1978), Sampling and observation of oceanic mantle and crust on Gorringe Bank, *Nature*, *273*, 45–49.

Bernard-Griffiths, J., G. Gruau, G. Cornen, B. Azambre, and J. Macé (1997), Continental lithospheric contribution to alkaline magmatism: Isotopic (Nd,Sr,Pb) and geochemical (REE) evidence from Serra de Monchique and Mount Ormonde complexes, *J. Petrol.*, *38*(1), 115–132.

Bogaard, P. v. d., H.-U. Schmincke, and A. Freundt (1988), Eruption ages and magma supply rates during the Miocene evolution of Gran Canaria, *Naturwissenschaften*, *75*, 616–617.

Bohrson, W. A., M. R. Reid, A. L. Grunder, M. T. Heizler, T. M. Harrison, and J. Lee (1996), Prolonged history of silicic peralkaline volcanism in the eastern Pacific Ocean, *J. Geophys. Res.*, *101*(B5), 11,475–11,474.

Cachao, M., D. Rodrigues, C. M. Silva, and J. Mata (1998), Biostratigrafia (Nanofosseis calcarios) e interpretacao paleoambiental do eogenico de Porto Santo (Madeira), V Congresso Nacional de Geologia, *Comun. Inst. Geologico Mineiro Lisboa*, *84*(1), A91–A94.

Cande, S. C., and Y. Kristoffersen (1977), Late Cretaceous magnetic anomalies in the North Atlantic, *Earth Planet. Sci. Lett.*, *35*, 215–224.

Carracedo, J. C. (1994), The Canary Islands: An example of structural control on the growth of large ocean-island volcanoes, *J. Volcanol. Geotherm. Res.*, *60*, 225–241.

Carvalho, G. d., and J. M. Brandão (1991), *Geologia do Arquipelago da Madeira*, Mus. Nac. de Hist. Nat., Lisbon.

Cornen, G. (1982), Petrology of the alkaline volcanism of Gorringe Bank (southwest Portugal), *Mar. Geol.*, *47*, 101–130.

Crisp, J. A. (1984), Rates of magma emplacement and volcanic output, *J. Volcanol. Geotherm. Res.*, *20*, 177–221.

Cyagor II Group (1984), Intraoceanic tectonism on the Gorringe Bank: Observations by submersible, in *Ophiolites and Oceanic Lithosphere*, edited by G. Gass, S. J. Lippard, and A. W. Shelton, pp. 113–120, Geol. Soc. of London, London.

Dalrymple, G. B., and W. A. Duffield (1988), High precision $^{40}Ar/^{39}Ar$ dating of Oligocene tephra from the Mogollon-Datil volcanic field using a continuous laser system, *Geophys. Res. Lett.*, *15*, 463–466.

Duffield, W. A., and G. B. Dalrymple (1990), The Taylor Creek Rhyolite of New Mexico: A rapidly emplaced field of domes and lava flows, *Bull. Volcanol.*, *52*, 475–478.

Duncan, R. A. (1981), Hotspots in the southern oceans—An absolute frame of reference for motion of the Gondwana continents, *Tectonophysics*, *74*, 29–42.

Dzurisin, D., R. Y. Koyanagi, and T. T. English (1984), Magma supply and storage at Kilauea volcano, Hawaii, *J. Volcanol. Geotherm. Res.*, *21*, 177–206.

Eckhardt, F. J., P. Müller, and H. Raschka (1975), Geochemische und petrologische Untersuchungen an Basalten der Meteor-Kuppenfahrt (Mittlerer Atlantik) (abstract), *Fortschr. Mineralog.*, *52*, Tagung der Sekt. Geochem. der Dtsch. Mineral. Ges., Karlsruhe, Germany.

Féraud, G., H.-U. Schmincke, J. Lietz, J. Gastaud, G. Pritchard, and U. Bleil (1981), New K-Ar ages, chemical analyses and magnetic data of rocks from the sland of Santa Maria (Azores),Porto Santo and Madeira (Madeira Archipelago) and Gran Canaria (Canary Islands), *Bull. Volcanol.*, *44*(3), 359–375.

Féraud, G., J. Gastaud, J.-M. Auzende, J.-L. Olivet, and G. Cornen (1982), $^{40}Ar/^{39}Ar$ ages for alkaline volcanism and the basement of Gorringe Bank, North Atlantic Ocean, *Earth Planet. Sci. Lett.*, *57*, 211–226.

Féraud, G., D. York, C. Mével, G. Cornen, C. M. Hall, and J.-M. Auzende (1986), Additional ^{40}Ar-^{39}Ar dating of the basement and the alkaline volcanism of Gorringe Bank (Atlantic Ocean), *Earth Planet. Sci. Lett.*, *79*, 255–269.

Ferreira, M. P., and J. Cotelo Neiva (1997), Carta geologica de Portugal, Folha da Ilha de Porto Santo, Inst. Geol. e Minereiro, Lisbon.

Ferreira, M. P., R. Macedo, V. Costa, and J. H. Reynolds (1975), Rare-gas dating, II, Attempted uranium-helium dating of young volcanic rocks from the Madeira Archipelago, *Earth Planet. Sci. Lett.*, *25*, 142–150.

Gerlach, D. C. (1990), Eruption rates and isotopic systematics of ocean islands: Further evidence for small-scale heterogeneity in the upper mantle, *Tectonophysics*, *172*, 273–289.

Hoernle, K., and H.-U. Schmincke (1993a), The petrology of the tholeiites through melilite nephelinites on Gran Canaria, Canary Islands: Crystal fractionation, accumulation and depths of melting, *J. Petrol.*, *34*, 573–597.

Hoernle, K., and H.-U. Schmincke (1993b), The role of partial melting in the 15 Ma geochemical evolution of Gran Canaria: A blob model for the Canary hotspot, *J. Petrol.*, *34*, 599–626.

Hoernle, K., G. Tilton, and H.-U. Schmincke (1991), Sr-Nd-Pb isotopic evolution of Gran Canaria: Evidence for shallow enriched mantle beneath the Canary Islands, *Earth Planet. Sci. Lett.*, *106*, 44–63.

Hoernle, K., Y.-S. Zhang, and D. Graham (1995), Seismic and geochemical evidence for largescale mantle upwelling beneath the eastern Atlantic and western and central Europe, *Nature*, *374*, 34–39.

Holik, J. S., and P. D. Rabinowitz (1991), Effects of the Canary hotspot volcanism on structure of oceanic crust off Morocco, *J. Geophys. Res.*, *96*, 12,039–12,067.

Keken, P. v. (1997), Evolution of starting mantle plumes: A comparison between numerical and laboratory models, *Earth Planet. Sci. Lett.*, *148*, 1–11.

Klügel, A., K. Hoernle, H.-U. Schmincke, and J. D. L. White (1999), The chemically zoned 1949 eruption on La Palma (Canary Islands): Petrologic evolution and magma supply dynamics of a rift zone eruption, *J. Geophys. Res.*, in press.

Litvin, V. M., V. V. Matveyenkov, E. L. Onishchenko, M. V. Rudenko, and A. M. Sagalevich (1982), New data on the structure of Ampère Seamount, *Oceanology*, *22*(1), 62–64.

Luongo, G., E. Cubellis, F. Obrizzo, and S. M. Petrazzuoli (1991), A physical model for the origin of volcanism of the Tyrrhenian margin: The case of the Neapolitan area, *J. Volcanol. Geotherm. Res.*, *48*, 173–185.

Marova, N. A., and Y. D. Yevsyukov (1987), The geomorphology of the Ampère submarine seamount (in the Atlantic Ocean), *Oceanology*, *27*(4), 452–455.

Mata, J., T. Boski, A. Boven, and J. Munhá (1995), Geochronologia das lavas da Madeira: Novas dataçoes K-Ar, *Gaia*, *11*, 53–56.

Matveyenkov, V. V., S. G. Poyarkov, O. V. Dmitriyenko, A. I. Al'Mukhamedov, G. R. Gamsakhurdia, and O. L. Kuznetsov (1994), Geological particularities of the seamount structure in the Azoro-Gibraltar Zone, *Oceanology*, *33*(5), 664–673.

McIntyre, R. M., and G. W. Berger (1982), A note on the geochronology of the Iberian Alkaline Province, *Lithos*, *15*, 133–136.

Mitchel-Thomé, R. C. (1976), *Geology of the Middle Atlantic slands*, *Borntraeger*, Berlin.

Morgan, W. J. (1972), Plate motions and deep mantle convection, *Mem. Geol. Soc. Am.*, *132*, 7–22.

Morgan, W. J. (1981), Hotspot tracks and the opening of the Atlantic and Indian Oceans, in *The Sea: Oceanic Lithosphere*, vol. 7, edited by C. Emiliani, pp. 443–487, John Wiley, New York.

Morgan, W. J. (1983), Hotspot tracks and the early rifting of the Atlantic, *Tectonophysics*, *94*, 123–139.

O'Conner, J. M., P. Stoffers, P. v. d. Bogaard, and M. McWilliams (1999), First seamount age evidence for significantly slower African plate motion since 19 to 30 Ma, *Earth Planet. Sci. Lett.*, *171*, 575–589.

Peirce, C., and P. J. Barton (1991), Crustal structure of the Madeira-Tore Rise, eastern North Atlantic—Results of a DOBS wide-angle and normal incidence seismic experiment in the Josephine Seamount region, *Geophys. J. Int.*, *106*, 357–378.

Pitman, W., and M. Talwani (1972), Sea floor spreading in the North Atlantic, *Geol. Soc. Am. Bull.*, *83*(3), 619–646.

Pollitz, F. F. (1991), Two-stage model of African absolute motion during the last 30 million years, *Tectonophysics*, *194*, 91–106.

Purdy, G. M. (1975), The eastern end of the Azores-Gibraltar Plate Boundary, *Geophys. J. R. Astron. Soc.*, *43*, 973–1000.

Schmincke, H.-U. (1982), Volcanic and chemical evolution of the Canary Islands, in *Geology of the Northwest African Margin*, edited by E. Seibold, pp. 273–306, Springer-Verlag, New York.

Schmincke, H.-U. (1998), Zeitliche, strukturelle und vulkanische Entwicklung der Kanarischen Inseln, der Selvagens Inseln und des Madeira-Archipels, in *Handbuch der Reptilien und Amphibien Europas*, edited by W. Bischoff, pp. 27–69, Aula Verlag, Wiesbaden, Germany.

Schmincke, H.-U., and H. Staudigel (1976), Pillow lavas on central and eastern Atlantic Islands (La Palma, Gran Canaria, Porto Santo, Santo Maria), *Bull. Soc. Geol. Fr.*, *7*(4), 871–883, (Preliminary report).

Schmincke, H.-U., and M. Sumita (1998), Volcanic evolution of Gran Canaria reconstructed from apron sediments: Synthesis of VICAP project drilling, *Proc. Ocean Drill. Program Sci. Results*, *157*, 443–469.

Smith, W. H. F., and D. T. Sandwell (1997), Global seafloor topography from satellite altimetry and ship depth soundings, *Science*, *277*, 1956–1962.

Stuiver, M., and P. Reimer (1993), Extendet ^{14}C data base and revise calib 3.0 ^{14}C program, *Radiocarbon*, *35*, 215–230.

Verhbitsky, E. V., and V. G. Zolotarev (1989), Heat flow and the Eurasian-African plate boundary in the eastern part of the Azores-Gibraltar fracture zone, *J. Geodyn.*, *11*, 267–273.

Walker, G. P. L. (1987), The dike complex of Koolau volcano, Oahu: Internal structure of a Hawaiian rift zone, in *Volcanism in Hawaii*, vol. 1350, edited by R. W. Decker, T. W. Wright, and P. H. Stauffer, pp. 961–993, U.S. Geol. Surv. Prof. Pap.

Watkins, N. D., and A. Abdel-Monem (1971), Detection of the Gilsa geomagnetic polarity event on the Island of Madeira, *Geol. Soc. Am. Bull.*, *82*, 191–198.

Wendt, I., and C. Carl (1991), The statistical distribution of the mean squares weighted deviation, *Chem. Geol.*, 86, 275–285.

Wendt, I., P. Kreuzer, and P. Müller (1976), K-Ar age of basalts from Great Meteor and Josephine seamounts (eastern North Atlantic), *Deep Sea Res. Oceanogr. Abstr.*, *23*(9), 849–862.

Werner, R., K. Hoernle, P. v. d. Bogaard, C. Ranero, R. v. Huene, and D. Korich (1999), A drowned 14 Ma old Galápagos Archipelago off the coast of Costa Rica: Implications for evolutionary and tectonic models, *Geology*, *27*, 499–502.

York, D. (1969), Least squares fitting of a straight line with correlated errors, *Earth Planet. Sci. Lett.*, *5*, 320–324.

Young, H. D. (1962), *Statistical Treatment of Experimental Data*, vol. 88, pp. 5101–5112, McGraw-Hill, New York.

Zbyszewski, G., A. Candido de Medeiros, O. d. Veiga Ferreira, and C.Torrede Assunçao (1973), Carta Geologica de Portugal 1/50,000, Noticia Explicativa da Folha Ilhas Desertas, Serv. Geol. de Portugal, Lisbon.

Zbyszewski, G., O. d. Veiga Ferreira, A. Candido de Medeiros, L. Aires-Barros, L. C. Silva, J. M. Munha, and F. Barriga (1975), Carta Geologica de Portugal 1/50,000, Noticia Explicativa das Folhas A e B da Ilha da Madeira, Serv. Geol. de Portugal, Lisbon.

Zhang, Y.-S., and T. Tanimoto (1992), Ridges, hotspots and their interaction as observed in seismic velocity maps, *Nature*, *355*, 45–49.